Chem

CellPress

Article

Supramolecular repair of hydration lubrication surfaces

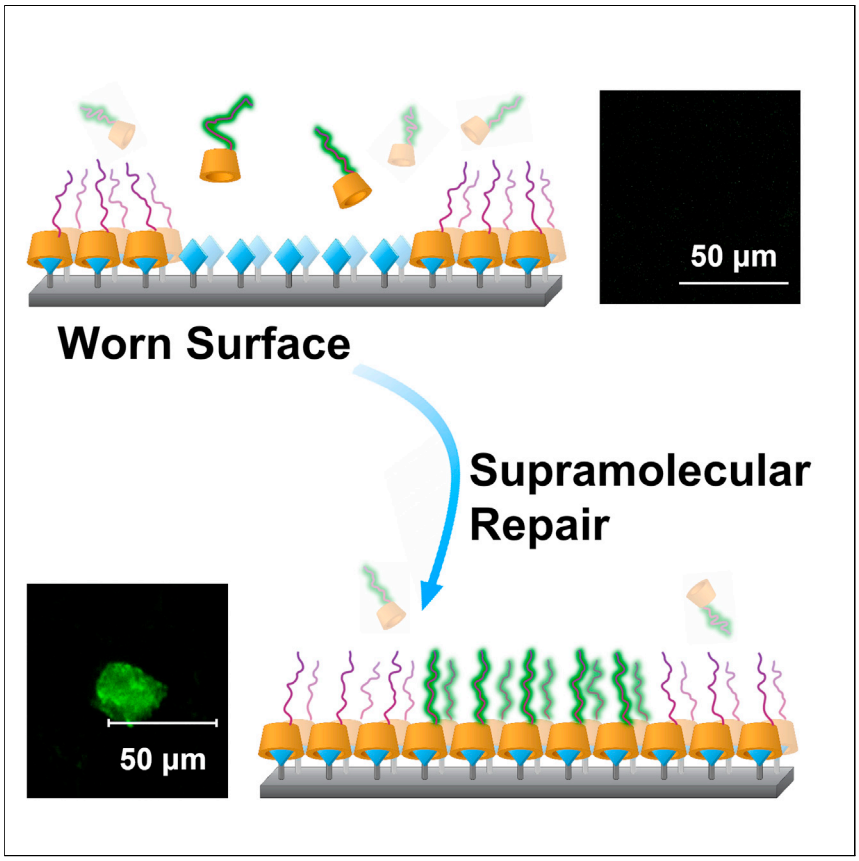

We propose the use of selective host-guest interactions to assemble lubricating polymers on functionalized surfaces. The concept is demonstrated using a cyclodextrin-terminated lubricating polymer that associates with an adamantane-functionalized surfaces. Areas of the surface that are damaged by mechanical wear are repaired as more lubricating polymer self-assembles with the surface. Low-friction surfaces that can be easily repaired are needed to limit energy losses and damage in biomedical and mechanical devices.

Yixin Wang, Yulong Sun, Alyssa-Jennifer Avestro, Paul R. McGonigal, Hongyu Zhang

paul.mcgonigal@durham.ac.uk (P.R.M.)
zhanghyu@tsinghua.edu.cn (H.Z.)

Highlights

Selective host-guest recognition leads to self-assembled polymer monolayers

The surfaces exhibit hydration lubrication, leading to low coefficients of friction

Wear and dynamic monolayer repair are visualized by confocal laser microscopy

Lubricity is restored *in situ* as supramolecular "weak links" are re-established

Wang et al., Chem *8*, 1–14
February 10, 2022
https://doi.org/10.1016/j.chempr.2021.11.001

Please cite this article in press as: Wang et al., Supramolecular repair of hydration lubrication surfaces, Chem (2021), https://doi.org/10.1016/j.chempr.2021.11.001

Chem

CellPress

Article

Supramolecular repair of hydration lubrication surfaces

Q1 Yixin Wang,[1,4] Yulong Sun,[1,2,4] Alyssa-Jennifer Avestro,[2,3] Paul R. McGonigal,[2,5,*] and Hongyu Zhang[1,*]

SUMMARY

Although advances in coating technologies have allowed us to match—or even exceed—the lubricity of Nature's low-friction surfaces, the performance of synthetic materials inevitably diminishes over time as the surfaces are worn and damaged by irreversible breakage of covalent bonds. Synthetic systems lack the bespoke repair mechanisms that replenish hydration lubrication surfaces in Nature. Here, we demonstrate dynamic repair of low-friction surfaces prepared through a surface-selective self-assembly strategy. Monolayers of lubricating polymers associate with functionalized surfaces through strong and specific host-guest interactions, leading to hydration lubrication surfaces with low coefficients of friction (0.024–0.028). Following friction-induced dissociation of the polymers, the polymer-to-surface interaction is restored by the reformation of host-guest complexes, thus repairing the monolayer, renewing the lubricity, and reducing the effects of wear. Such dynamically restored low-friction materials will be an essential tool in decreasing Q2 **global energy use—a fifth of which is expended overcoming friction.**

The bigger picture

Friction between contacting surfaces reduces energy efficiency and causes irreversible damage, leading to an estimated 20% of global energy consumption. Natural systems minimize friction by (1) exploiting surfaces that attract a lubricating layer of water molecules and (2) replenishing surfaces as they become worn. Here, we outline a strategy to obtain synthetic coatings that exhibit both of these desirable characteristics. We make use of selective supramolecular interactions to dynamically assemble a lubricating polymer on a surface. These attractive interactions restore the lubricating surface *in situ* following periods of mechanical wear. This "supramolecular repair" concept could be expanded upon using diverse recognition motifs, surface chemistries, or polymer structures to achieve low-friction coatings. Such coatings may enhance the lifetimes and the efficiencies of articulating components in biomedical and mechanical systems.

Q3 Q4 Q5 Q6 INTRODUCTION

Low-friction materials that have evolved in Nature, such as the articulating cartilage surfaces found in healthy human joints,[1,2] exhibit remarkably low coefficients of friction (COFs). In many cases, they attain their low COFs as a result of hydration lubrication.[3,4] Layers of water molecules, which are tightly bound to the lubricating surfaces, relax rapidly when subjected to shear, minimizing drag and giving COFs down to 0.001.[3] Synthetic low-friction materials that draw inspiration from the high-lubricity surfaces in Nature have become central to the investigation of fundamental interfacial phenomena and to technological applications, where their low sliding resistance and minimal wear limit energy waste and prevent premature mechanical failure.[1,5]

Beyond lubricity, ideal low-friction surfaces should also possess (1) sufficient malleability to dissipate compressive stress,[6] (2) high resistance to mechanical wear and surface degradation over extended periods of shear and repeated impact events, as well as (3) a simple means of repair for when degradation inevitably occurs by the breakage (Figure 1A) of covalent bonds. Robust low-friction materials, such as poly(tetrafluoroethylene) (i.e., Teflon), graphene,[8] and diamond-like carbon,[9] are available but have inherently high stiffnesses, which hinders their use in articulating materials and at soft interfaces.[10] Soft, easily reparable, low-friction surface coatings are needed in the context of, for example, artificial hip joints,[11–13] whose wear over time (Figure 1A) can lead to complications requiring further medical treatment. Therefore, in recent years, research has been directed toward soft surface coatings that meet criteria (1)–(3).

Please cite this article in press as: Wang et al., Supramolecular repair of hydration lubrication surfaces, Chem (2021), https://doi.org/10.1016/j.chempr.2021.11.001

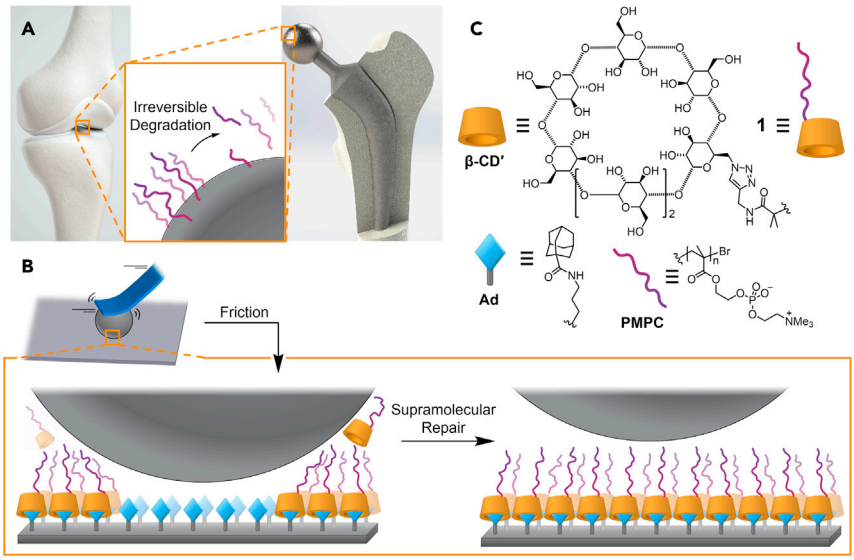

Figure 1. Illustration of the differences between irreversible wear of a covalently functionalized surface and dynamic repair of a reversibly assembled lubricating layer

(A and B) (A) Natural cartilage and artificial hip joints can be lubricated by covalently attached (bio) polymer layers, which undergo irreversible mechanical wear through breakage of covalent bonds, whereas (B) a surface-bound layer of lubricating β-CD′-PMPC polymer, **1**, is restored upon reforming noncovalent bonds with surface-bound Ad units after friction-induced dissociation. An idealized monolayer is shown for simplicity. A mixture of vacant sites and mushroom-like and brush-like polymer domains are likely present at equilibrium.

(C) Structural formulas of the components of the hydration lubrication surface. Ad is connected to a Ti surface through a silane linkage.[7]

Compressible hydration lubrication surface coatings have been prepared from a variety of synthetic materials—surfaces have been coated with non-specific adsorbents, such as liquid surfactants[3] and bio-mimetic lipid bilayers,[14] or covalently functionalized with (super)hydrophilic polymer brushes.[10,15,16] Zwitterionic poly(2-methacryloyl-oxyethyl phosphorylcholine) (PMPC) materials[10] perform particularly well, recruiting the layer of water molecules needed to enact hydration lubrication and achieving record-low (<0.001)[3,17] COFs in certain cases. Yet, state-of-the-art hydration lubrication surfaces and other biocompatible low-friction materials currently lack robustness or an ability to repair dynamically in a prescribed manner. Indeed, self-healing boundary lubricants have been developed based on immiscible fluid layers immobilized on porous surfaces,[18] ionogels,[19] and microcapsule-impregnated polymers.[20] However, in general, there has been a dichotomy between high-wear resistance and flexibility, while limited progress has been made[21] toward simple surface-repair mechanisms that could operate in biologically relevant settings. Progress is needed in this area to minimize the irreversible degradation of covalently bound surface layers that inevitably occurs (Figure 1A) when surfaces are subject to repeated wear.

Here, we report the design, synthesis, and investigation of dynamically repairing hydration lubrication surfaces based on the self-assembly of polymer monolayers through strong and specific host-guest interactions that operate in water. When friction is applied to the surfaces, the host-guest complexes, which serve as pre-programmed weak links, dissociate preferentially. We show that surfaces can recover from mechanical wear by reformation of the noncovalent bonding interactions, which, in turn, restores lubricity.

[1]State Key Laboratory of Tribology, Department of Mechanical Engineering, Tsinghua University, Beijing 100084, China

[2]Department of Chemistry, Durham University, Lower Mountjoy, Durham DH1 3LE, UK

[3]Department of Chemistry, University of York, Heslington, York YO10 5DD, UK

[4]These authors contributed equally

[5]Lead contact

*Correspondence: paul.mcgonigal@durham.ac.uk (P.R.M.), zhanghyu@tsinghua.edu.cn (H.Z.)

https://doi.org/10.1016/j.chempr.2021.11.001

Please cite this article in press as: Wang et al., Supramolecular repair of hydration lubrication surfaces, Chem (2021), https://doi.org/10.1016/j.chempr.2021.11.001

RESULTS AND DISCUSSION

Molecular design and synthesis

We sought to develop a strategy for incorporating a low-friction coating onto surfaces by taking advantage of the dynamic reversibility and specificity of host-guest interactions. We hypothesized that such interactions between a guest-decorated surface and a host-functionalized lubricating polymer would enable the surface to recover from damage (Figure 1B) through reversible supramolecular assembly, which would be helpful in circumventing the effects of mechanical wear. The biocompatible and bioorthogonal[22,23] interaction of macrocyclic β-cyclodextrin (β-CD) hosts with adamantyl guests[24–26] has been successfully applied to generate self-healing hydrogels,[27–31] to prepare self-assembled monolayers,[32–35] and to organize polymers on the surface of vesicles.[36] Adamantyl guests are well matched to the hydrophobic cavity of β-CD, typically giving rise to high association constants, K_a, of ~3 × 10^4 M^{-1} in aqueous solution.[24] Therefore, compound 1 was identified (Figure 1C) as a suitable target. It incorporates a β-CD macrocycle derivative (β-CD′) at the terminus of a PMPC backbone, enabling highly selective interactions with surface-bound 1-adamantane carboxamide (Ad) residues.

We prepared **1** in two steps from propargyl 2-bromo-2-methylpropionamide (BMP). In the first step, a 2-methacryloyloxyethyl phosphorylcholine (MPC) monomer was subjected to atom-transfer radical polymerization (ATRP) conditions using BMP as the initiator, which afforded an alkyne-terminated polymer. See the Methods and supplemental information for detailed procedures. A Cu(I)-catalyzed azide-alkyne cycloaddition (CuAAC) reaction with mono-(6-azido-6-deoxy)-β-cyclodextrin was used to link the terminus of the polymer to the primary rim of β-CD′, giving **1**. We also prepared a fluorescein-tagged analog, **1′**, by copolymerizing a 1:14 ratio of fluorescein *O*-methacrylate monomer with MPC before subjecting the resulting alkyne to the same CuAAC conditions. Both lubricating polymers **1** and **1′** have been structurally characterized by Fourier transform infrared (FTIR), fluorescence, and nuclear magnetic resonance (NMR) spectroscopies, as well as size-exclusion chromatography (SEC). See the supplemental information. The SEC data (Table S3) reveal a multimodal distribution of polymers **1** and **1′** in which the major components possess molecular weights of 297 and 59.1 kDa, respectively. The polydispersities measured (1.3–1.6) are a consequence of the mixed solubility profiles of the charged intermediates produced during polymerization.

Surface functionalization

In order to probe the lubricating and dynamic self-assembly properties of **1**, we functionalized the surface of Ti-6Al-4V (Ti) wafers with Ad groups that complement the β-CD′ end group of the PMPC. First, alkylamine-functionalized substrates, **Ti-NH$_2$**, were prepared by treating Ti wafers with aminopropyltriethoxysilane (APTES).[7] We verified the presence of primary alkylamino groups on the surfaces by performing (Figure 2) attenuated total reflection (ATR) FTIR analysis and X-ray photoelectron spectroscopy (XPS), observing (1) absorbances at 3,352 and 3,282 cm^{-1} that arise (Figure 2A) from symmetrical and asymmetrical stretching vibrations of NH_2 groups[37] and (2) photoelectrons in the N1s region with a binding energy of 398 eV, indicative (Figure 2B) of a single N-atom environment. The **Ti-NH$_2$** wafers were further functionalized by treating with 1-adamantanecarboxylic acid chloride in order to covalently connect (Figure 1C) Ad residues to the surfaces. XPS analysis of the resulting **Ti-Ad** substrates shows that a significant proportion of the **Ti-NH$_2$**-reactive sites are converted to Ad groups. Peak fitting of the C1s region of the **Ti-Ad** spectrum reveals (Figure 2B) the emergence of a shoulder at ~288 eV, which

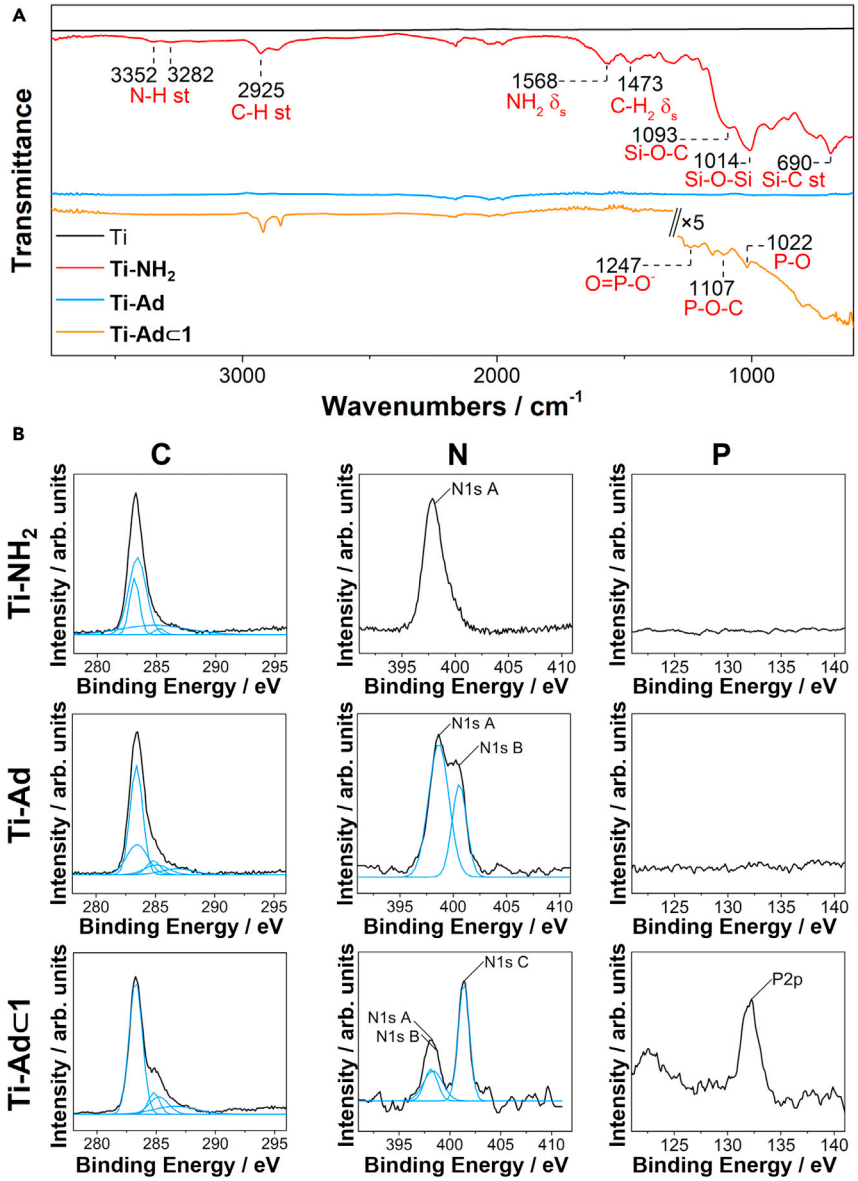

Figure 2. Characterization of functionalized Ti-NH_2, Ti-Ad, and Ti-Ad⊂1 wafers

(A) ATR-FTIR spectra.

(B) X-ray photoelectron spectra with peak-fitting traces shown in blue. FTIR signals of **Ti-Ad⊂1** below 1,300 cm^{-1} are magnified by a factor of 5.

matches the binding energy expected for an amide C environment[38] and has low intensity in keeping with its low abundance relative to alkyl C atoms. Two signals can be distinguished at 398 and 400 eV in the N1s region, which suggest the presence of N atoms in two bonding environments. Therefore, the N and C signals are consistent with a mixture of adamantane carboxamide linkages and unreacted amine groups being present on the surface. The signal at 398 eV, which we assign as the primary amine by comparison with XPS of **Ti-NH_2**, accounts for 67% of the peak area, indicating an amine-amide ratio of 2:1.

The lubricating surface layer was assembled by submerging a **Ti-Ad** wafer in a 10 mg/mL aqueous solution of **1** at room temperature. Under these conditions,

Please cite this article in press as: Wang et al., Supramolecular repair of hydration lubrication surfaces, Chem (2021), https://doi.org/10.1016/j.chempr.2021.11.001

the self-assembling system reaches equilibrium over approximately 2 h (vide infra). We immersed the wafer in the solution of **1** for 12 h to ensure the surface coating had fully equilibrated. After removing the wafer from the solution, it was rinsed with deionized water and the surface was analyzed to detect the surface-bound polymer. The ATR-FTIR spectrum of this wafer, **Ti-Ad⊂1**, exhibits (Figure 2A) absorbances typical of phosphate groups in the 1,000–1,250 cm^{-1} region of the infrared spectrum and XPS analysis shows (Figure 2B) additional signals in the N1s and P2p regions, as would be expected for a surface coated with the phosphorylcholine groups of **1**. The P signal at 132 eV appears as an asymmetric peak as a consequence of its overlapping P2p3/2 and P2p1/2 components, which is typical for phosphates.[38] Therefore, these measurements show that the **Ti-Ad⊂1** wafer retains adsorbed **1** after rinsing with water as a result of the noncovalent bonding interactions between the polymer and the surface. Assembly of **1** on a similarly functionalized **Ti-Ad** surface of a quartz crystal microbalance (QCM) sensor was also measured, revealing (Table S5) a surface coverage of 1.8 $pmol \cdot cm^{-2}$ that is consistent with a mushroom-like surface monolayer of adsorbed polymer.

Friction properties

We investigated the nanotribological properties of the surfaces under ambient conditions. First, we used atomic force microscopy (AFM) to measure (Figure S18) the adhesion forces between a β-CD-modified polystyrene-microsphere AFM tip (Figure S15) and the Ti surfaces immersed in water.[39] Although the **Ti-Ad⊂1** substrate and an unmodified Ti substrate exhibit similar adhesive forces (37 and 49 nN, respectively) when brought into contact with the β-CD-coated tip, the **Ti-Ad** substrate experiences a significantly larger adhesive force of 262 nN. We attribute this difference to the strong and specific noncovalent bonding interactions that develop between the macrocyclic hosts of the tip and the free Ad guests of the **Ti-Ad** surface.[40,41] The apparent lack of these interactions between the AFM tip and the **Ti-Ad⊂1** surface suggest that the Ad groups of **Ti-Ad⊂1** are largely occupied, rendering them essentially unavailable to bind the β-CD macrocycles of the AFM tip. This observation illustrates the selectivity of the assembly process—a surface lacking free Ad groups does not interact strongly with the end groups present in polymer 1.

Next, using a 5 μm-diameter polystyrene-microsphere AFM tip coated with PMPC[42] (Figure 3, inset), we carried out friction force measurements with alternant loads of 400 and 500 nN applied (Figure 3) to the surfaces, giving contact pressures >54 MPa to simulate the pressures experienced by hip joints during exercise.[43] Microscopic friction forces were measured by scanning the PMPC-coated AFM tip at a frequency of 2 Hz across a sliding area of 20 × 20 μm for 2 min while the surfaces were immersed in either pure water or a 10 mg/mL aqueous solution of **1**. This concentration optimizes performance without exceeding the solubility limit of the polymer (Table S4). Literature COF values for two interacting PMPC-coated surfaces in water—where each surface is covalently functionalized with a polymer monolayer—are typically in the range of 0.01–0.05 on account of efficient hydration lubrication[44–46] and can be extended to as low as 0.001 for highly optimized systems.[3,4] In our investigation, the largest friction forces were measured (Figure 3) when the PMPC-coated AFM tip was applied to an unmodified Ti surface in pure water, giving rise to a COF of 0.264. Employing an aqueous 10 mg/mL solution of **1** as the medium reduces the COF 5-fold to 0.044 by virtue of the additional hydration lubrication provided by weakly adsorbed polymer molecules on the Ti surface and polymer present in the medium immediately surrounding the contacting surfaces.[3] Covalent modification of the Ti surface with primary amine and Ad residues also reduces friction—although it does so to a lesser extent. The **Ti-Ad** substrate exhibits a COF of 0.067

Please cite this article in press as: Wang et al., Supramolecular repair of hydration lubrication surfaces, Chem (2021), https://doi.org/10.1016/j.chempr.2021.11.001

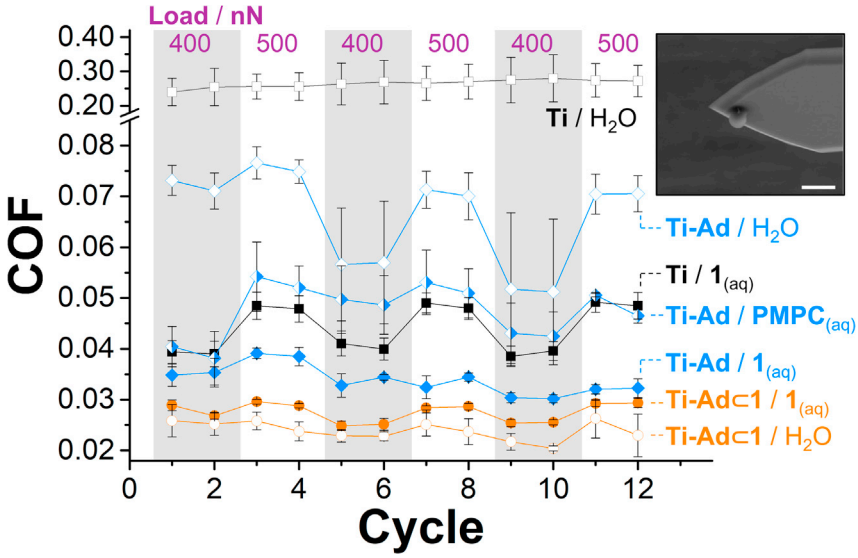

Figure 3. Friction force performances measured by AFM in contact mode show that the optimum COF is obtained when all components of the self-assembling system are present

The COF is derived by dividing the lateral force observed by the normal force applied. Measurements were performed on surfaces immersed in either pure H_2O, represented by hollow data points, a solution of PMPC in H_2O (10 mg/mL), shown by half-filled data points, or a solution of **1** in H_2O (10 mg/mL), shown with filled data points. The gray and white areas of the plot correspond to cycles performed using AFM-tip normal forces of 400 and 500 nN, respectively. Error bars show the standard deviation over three samples. **Inset**. SEM image of the PMPC-coated polystyrene-microsphere AFM tip. Scale bar, 10 μm.

in pure water. Exposing the **Ti-Ad** substrate to a 10 mg/mL aqueous solution of PMPC lacking a β-CD head group lowers the COF slightly to 0.047 on account of non-selective adsorption of the polymer to the Ad surface. However, importantly, we observe the lowest COF values for our substrates when all components of the host-guest system are present. A **Ti-Ad** wafer freshly immersed in the solution of **1** exhibits a COF of 0.034—a 2-fold improvement relative to the COF measured for the same surface in the absence of the host-functionalized polymer. The COF is further improved to 0.024–0.028 when a pre-complexed substrate, **Ti-Ad⊂1**, is used (Figure 3) in place of the **Ti-Ad** wafer in either H_2O or the solution of **1**, suggesting that the lubricity of the surface increases when the self-assembly of the surface layer has fully equilibrated. Indeed, the lubricities of the equilibrated **Ti-Ad⊂1** substrate measured (Figure 3) in H_2O and $\mathbf{1}_{(aq)}$ are similar to one another, which is consistent with the surface-bound layer of **1** present on the **Ti-Ad⊂1** substrate resisting dissociation even when the surface is immersed in H_2O. The selectivity of the noncovalent bonding interactions is evident when comparing the performance of the bare Ti and **Ti-Ad** substrates in the presence of **1**, where the guest-functionalized surface exhibits a significantly lower COF. Overall, the nanotribological experiments demonstrate that favorable host-guest interactions between the β-CD′ and Ad groups lead to a surface coating of phosphorylcholine groups being recruited by the Ti surface, which enacts hydration lubrication and reduces the overall drag experienced when the surface is rubbed.

Supramolecular repair of the lubricating surfaces

In order to investigate the ability of the self-assembled surface to be dynamically repaired when subjected to mechanical wear, we prepared two coated glass slides,

Please cite this article in press as: Wang et al., Supramolecular repair of hydration lubrication surfaces, Chem (2021), https://doi.org/10.1016/j.chempr.2021.11.001

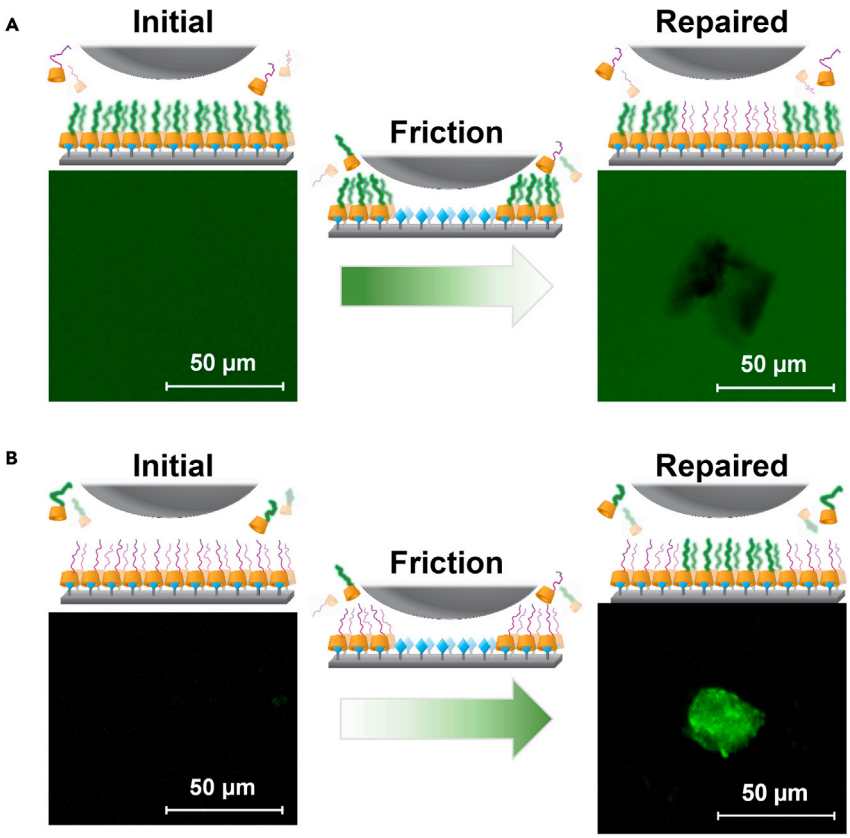

Figure 4. Confocal laser scanning microscope images of ~20 × 20 μm worn areas created by applying 400 nN normal force in AFM contact mode (polystyrene-microsphere tip) across glass slides

(A and B) (A) **Glass-Ad⊂1′** under a 10 mg/mL aqueous solution of **1** and (B) **Glass-Ad⊂1** under a 10 mg/mL aqueous solution of **1′**. An idealized monolayer structure is depicted for simplicity. Under the experimental conditions, worn areas will equilibrate (i.e., self-heal) to replicate the mixture of vacant sites and mushroom-like and brush-like polymer domains.

labeled **Glass-Ad⊂1** and **Glass-Ad⊂1′**, suitable for confocal laser scanning microscopy (CLSM) analysis. The slides were fabricated following procedures similar to those described for the preparation of the **Ti-Ad⊂1** substrates—functionalized **Glass-Ad** slides were prepared by covalent bond formation and then subjected to self-assembly conditions with either polymer **1**, to give **Glass-Ad⊂1**, or fluorescently labeled analog **1′**, giving **Glass-Ad⊂1′** (see supplemental information). The successful modification of the glass substrates is evident (Figure 4) by the uniform green emission visible from the **Glass-Ad⊂1′** surface by CLSM while irradiating with 485 nm laser light to excite the fluorescein chromophores of polymer **1′**, as well as XPS analysis (Figure S17). We subjected this **Glass-Ad⊂1′** substrate to mechanical wear by AFM while under a 10 mg/mL aqueous solution of non-emissive **1**, applying a 400 nN normal force through a bare polystyrene-microsphere tip in contact mode as it was repeatedly scanned across a 20 × 20 μm area at 2 Hz for 20 min. A bare polystyrene-microsphere tip was used to maximize wear—similar experiments performed with PMPC-coated tips did not cause a noticeable change in the surfaces over the course of the 20-min experiments. After wearing the **Glass-Ad⊂1′** slide with the bare polystyrene-microsphere tip, it was allowed to stand in the solution of **1** for 2 h. CLSM analysis of the surface shows (Figure 4A) that the worn area becomes non-emissive, which suggests that the fluorescent polymer **1′** has desorbed

Please cite this article in press as: Wang et al., Supramolecular repair of hydration lubrication surfaces, Chem (2021), https://doi.org/10.1016/j.chempr.2021.11.001

from the surface, being replaced by **1**. The reformation of β-CD′–Ad interactions restores the lubricating monolayer (vide infra). To better visualize the repair step and confirm that the surface is indeed repaired by assembly of polymer from solution, we conducted the converse experiment using a non-emissive **Glass-Ad⊂1** substrate immersed in a solution of the fluorescent polymer **1′**. Initially, the surface is non-emissive, but the worn area becomes fluorescent (Figure 4B) upon exchange of surface-bound **1** for **1′** from solution. The areas of the glass slide that have not been worn remain relatively non-emissive, illustrating that the desorption is accelerated (Figure S24) by the mechanical wearing process. Taken together, the exchange processes observed on **Glass-Ad⊂1** and **Glass-Ad⊂1′** substrates demonstrate that (1) in the absence of friction, the initially adsorbed polymer layer is metastable, desorbing partially over a 12-h period (Figure S24). There are not significant amounts of background desorption while the surfaces are immersed in solution over the 2-h timescale of the experiment, even in the presence of a competitive host molecule in the solvent medium. This observation is consistent with strong and selective interactions between the CD groups of **1** and the Ad-functionalized surface rather than weak, non-selective binding. Previously, Huskens et al. have observed similar metastability of densely packed monolayers formed by interactions of β-CD and multivalent Ad guests.[32,33] Our experiments also reveal that (2) the 400 nN normal force, which corresponds to a shear stress of 7.5 MPa at the COF for this surface of 0.138 (Figure 5) with the bare polystyrene-microsphere AFM tip, is sufficient to cause the noncovalently attached polymers to desorb from the surface but (3) does not significantly degrade the covalently bonded Ad sites of the modified glass substrates. As a result, (4) the surface is dynamically repaired by self-assembly of a fresh layer of lubricating polymer from the bulk solution as the favorable β-CD′–Ad interactions reform.

Finally, we investigated (Figure 5) whether repair of the self-assembled polymer layers also restores the lubricity of the surfaces. We wore a 20 × 20 μm patch of **Glass-Ad⊂1** substrate under pure water using a bare polystyrene-microsphere AFM tip with a normal force of 500 nN at 2 Hz for 30 min, ensuring that a significant quantity of the polymer would desorb. In the absence of dissolved polymer, the surface layer would not be expected to repair. Indeed, we observed that the COF between the substrate and bare polystyrene-microsphere AFM tip increased from an initial value of 0.138 for the self-assembled surface to 0.533 after being worn. The worn area was then immersed in a 10 mg/mL aqueous solution of **1** while intermittently performing friction force measurements under a normal force of 400 nN to monitor (Figure 5A) the change in COF over time as the surface is repaired. We observed that the lubricity is gradually restored on the minute-to-hour timescale, plateauing after approximately 2 h. This dynamic restoration of the **Glass-Ad⊂1** substrate returns the COF (Figure 5B) to 0.208.

The kinetics of the repair process are consistent with the kinetics of association observed by QCM (Figures 5C and 5D) and with the observed resistance of the fully equilibrated polymer layers to desorption[47] under ambient conditions, e.g., when the solvent medium is exchanged (Figure 4). The QCM measurements indicate that when a **Ti-Ad** surface is first exposed to $\mathbf{1}_{(aq)}$, the surface is rapidly coated with an initial layer of the polymer, reaching two-thirds of the eventual surface-bound polymer mass within 2 min. However, the mass of adsorbed polymer continues to increase gradually over a period longer than 30 min as the self-assembled monolayer equilibrates toward a more closely packed structure. Comparison with the lubricity over a similar period indicates (Figure 5A) that this closely packed PMPC layer is needed to impart a low COF.

Please cite this article in press as: Wang et al., Supramolecular repair of hydration lubrication surfaces, Chem (2021), https://doi.org/10.1016/j.chempr.2021.11.001

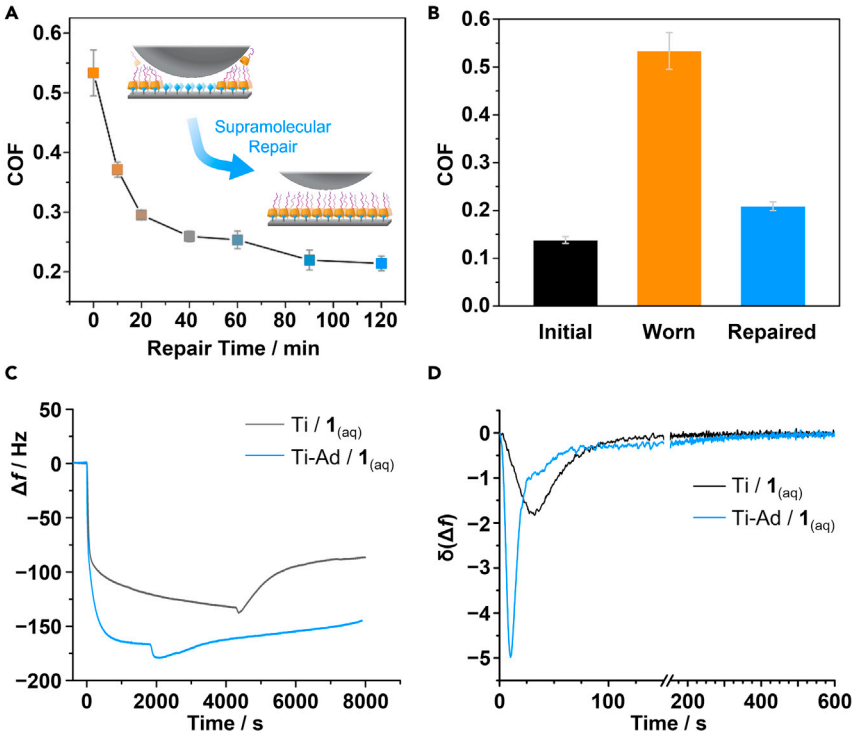

Figure 5. Supramolecular repair of the hydration lubrication polymer surface after wear-induced polymer desorption restores the COF to near its initial value

The COF was measured using a normal force of 400 nN applied through a bare polystyrene-microsphere tip.

(A) The COF of the worn area of a **Glass-Ad⊂1** slide decreases over time as it stands in a 10 mg/mL aqueous solution of **1**.

(B) Comparison of the COF before the surface is worn, after wearing in pure water for 20 min under a 500 nN normal force, and after subsequent healing in a solution of **1** for 2 h. Error bars in (A) and (B) show the standard deviation over three trials.

(C) QCM data showing adsorption of 10.0 mg/mL aqueous **1** on a chip with either a bare Ti surface or a **Ti-Ad** surface for the n = 3 overtone. Sample injection occurs after an initial equilibration with H_2O (set as t = 0 s) and proceeds at a flow rate of 100 $\mu L \cdot min^{-1}$ until a plateau in frequency is reached, before switching back to H_2O. The runs were performed up to a total of 8,000 s (~2.25 h). The changes in frequency immediately before switching back to H_2O (i.e., at the end of adsorption), $\Delta f_{solution}$, and at the end of the 8,000 s run after the rinsing period, Δf_{rinsed}, were used to calculate the mass densities shown in Table S5.

(D) Differentials of the data from (C), showing that **1** adsorbs to the **Ti-Ad** surface at a higher initial rate than to the bare Ti surface but that the bare Ti surface reaches a plateau in frequency more quickly.

Conclusions

A diverse set of technologies stand to benefit from improved low-friction materials, ranging from artificial biomedical implants[8–10] and micro- or nanoelectromechanical systems,[48] to energy-efficient vehicles.[49] Although optimization of absolute surface lubricity is clearly a primary consideration, the longevity of materials is also of paramount importance. Materials must perform over repeated cycles of operation, either by resisting degradation when subjected to mechanical wear or by employing mechanisms that replenish lubricating surface coatings. Nature's lubricating surfaces, such as the cartilage found in human joints, are replenished by biological machinery that reconstructs the covalent structures of self-assembling surface layers. We have demonstrated that a phenomenologically different repair strategy can achieve a

similar effect in synthetic materials, making use of simple molecular components—self-assembled surface coatings of lubricating polymers combat degradation by dynamic restoration of the surface structure, reversing the effects of mechanical wear and restoring lubricity. We have exemplified this concept using the noncovalent bonding interactions between a functionalized β-CD′ polymer and Ad groups in water. The self-assembly recruits a lubricating layer of PMPC to the surface, which friction force measurements have shown to perform similarly to other PMPC-based hydration lubrication systems. By contrasting the behavior of a fluorescently tagged polymer with the non-emissive analog and performing friction force measurements, we have shown that the self-assembled system undergoes exchange when worn. Mechanical wear breaks the noncovalent bonding interactions, which, on account of their inherent reversibility, then re-establish dynamically to repair the surface and restore lubricity. Although they are not as low as the most highly optimized covalent-link systems reported (0.001),[3,4] the COF values obtained by our weak-link supramolecular concept (0.024–0.028) are characteristic[44–46] and well within the range of established hydration lubrication systems (0.01–0.05). Unlike these established systems, our results demonstrate that the specificity of supramolecular host-guest interactions can be exploited to assemble a low-COF hydration lubrication layer that is simultaneously capable of dynamic repair. Future optimization and tuning of weak-link host-guest pairs will be required to match the lubricity of purely covalent surface coatings. In this proof-of-concept system, the self-assembled surface monolayer is remarkably resistant to desorption, exhibiting metastability on the timescale of several hours while submerged in water despite its assembly being driven by discrete, monovalent β-CD′–Ad interactions. The application of multivalent[35,50] surface-to-polymer interactions may further enhance the stability of the surface coating while allowing the friction-induced breakage and subsequent reformation of noncovalent bonding interactions to occur without complete dissociation. The biocompatibility and biorthogonality[22,23] of the components bode well for the application of this, or similar, surface-selective self-assembly systems in the context of artificial joint lubrication to extend the lifetimes of medical implants. By analogy to synthetic polymers that can be injected into synovial joints to treat osteoarthritis,[21] solutions of polymers exhibiting selective noncovalent bonding interactions with artificial joints could be employed to restore their hydration lubrication surfaces, mitigating the effects of enzymatic and friction-induced degradation. This selective self-assembly strategy may also be of broader applicability as part of more durable low-friction materials, which are needed to increase the energy efficiency of mechanical devices in general.

EXPERIMENTAL PROCEDURES

Resource availability

Lead contact

Further information and requests for resources should be directed to and will be fulfilled by the lead contact, Paul McGonigal (paul.mcgonigal@durham.ac.uk).

Materials availability

All unique/stable reagents generated in this study are available from the lead contact with a completed materials transfer agreement.

Data and code availability

The data that support the findings of this study are available from the corresponding authors upon reasonable request.

Materials and methods

MPC was supplied by *Joy-Nature Corp. (Nanjing, China)*. APTES, anhydrous toluene, propargylamine, trimethylamine, 2-bromopropionyl bromide, CuBr, CuI, *N*,*N*,*N*′,*N*″,*N*″-pentamethyldiethylenetriamine (PMDETA), and *tert*-butyl hydroperoxide were purchased from *J&K Scientific (Beijing, China)*. Amine-modified polystyrene microspheres (4.0–4.9 μm diameters) were purchased from *Aladding (Shanghai, China)*. The "TL-CONT" variety of tipless AFM cantilever probe was purchased from *NanoWorld AG (Geneva, Switzerland)*. Ti wafer (10 × 10 mm, Ti-6Al-4V) was purchased from *Goodfellow (London, England)*. Petroleum ether, ethanol, acetone, tetrahydrofuran (THF), and *N*,*N*-dimethylformamide (DMF) were purchased from *Modern Oriental* Technology Development (Beijing, China). NMR spectra were recorded by using an Ascend 400 MHz spectrometer or Ascend 800 MHz spectrometer from *Bruker, Billerica, USA*. ATR-FTIR spectra were recorded by using a Nicolet FTIR 6700 instrument (*Thermo Fisher Scientific Waltham, USA*) fitted with an ATR module. XPS data were recorded using an X-ray photoelectron spectrometer (*PHI Quantera II, Bruker, Billerica, USA*) equipped with a 15 kV Mg-Kα radiation source. The take-off angle of the photoelectrons was maintained at 90°, and five scans were taken for each sample. Friction experiments were accomplished by using an MFP-3D Classic atomic force microscope *from Oxford Instruments Asylum Research, Santa Barbara, CA, USA*.

Friction performance measurements

Normal and friction force measurements were performed on the *Asylum Research* MFP-3D AFM in contact mode. The spring constant of the TL-CONT probe was determined by the frequency method,[51] and the lateral sensitivity of the probe was obtained by the improved wedge calibration method before the measurement.[52,53] The friction tests were performed at room temperature, over a sliding area of 20 × 20 μm, at a sliding angle of 90°, and frequency of 2 Hz, using a PMPC-coated AFM tip (see further on for preparation details). In order to simulate the pressure that hip joint undergo during strenuous exercise,[48] we choose two different normal forces under which the pressure of contact area exceeds the actual contact pressure[43] in natural hip joint, i.e., 2.6 MPa (see supplemental information). Either pure water or a 10 mg/mL aqueous solution of **1** were used as the lubricant. During the test, three random areas of 20 × 20 μm were chosen to carry out friction tests in each group. Each area was subjected to three successive cycles of normal force through stages of two scans each at 400 nN then 500 nN. Each normal force in the cycles was applied to scan the whole 20 × 20 μm area once in 128 s (256 lines per area and scan rate of 2 Hz). The surface roughness of the Ti and glass surfaces were characterized by AFM (Figures S19–S23).

Surface-repair experiments

Dynamic repair properties were characterized by applying a friction force to a substrate by AFM using a bare polystyrene-microsphere AFM tip, then examining the surface using CLSM. In order to observe wear area by CLSM, we used coated glass slides that were prepared by the same method used to functionalize the Ti-6Al-4V wafers (see supplemental information). During the friction experiments, **Glass-Ad⊂1** was worn under the normal force of 500 nN of a colloidal polystyrene-microsphere AFM tip for 30 min, then 200 μL of 10 mg/mL $\mathbf{1}_{(aq)}$ solution was added onto the slide to allow the worn area to repair. The COF of the worn area was measured at regular intervals by AFM (normal force: 400 nN, sliding distance: 20 μm, scan area: 20 × 20 μm, scan rate: 2 Hz). To visualize the polymer desorption and subsequent restoration, a **Glass-Ad⊂1′** slide was worn under 10 mg/mL of $\mathbf{1}_{(aq)}$ solution and **Glass-Ad⊂1** was worn under 10 mg/mL of $\mathbf{1'}_{(aq)}$ solution. The slides were worn at

room temperature under the same experimental conditions as before (wearing under a normal force of 500 nN using a bare polystyrene-microsphere AFM tip for 30 min).

Preparation of Ti-Ad wafers

The surfaces of commercially sourced Ti-6Al-4V wafers were first cleaned by ultrasonication in pure water and acetone for 5 min and dried under nitrogen flow. Then the cleaned wafers were functionalized with amine groups by silanization of the Ti surface using APTES. Adamantane groups were then grafted onto the surfaces by acylation of the amines with 1-adamantanecarboxylic acid chloride. For specific experimental details, see the supplemental information (Scheme S6).

Synthesis of 1 and 1′

1 was prepared by a three-step method shown in Schemes S1, S2, and S4 of the supplemental information. Briefly, BMP was synthesized by amidation of 2-bromopropionyl bromide with propargyl amine (Scheme S1) then used as an initiator to synthesize an alkynyl-terminated-PMPC polymer (alkynyl-PMPC) through ATRP (Scheme S2) of MPC. The alkynyl-PMPC was modified via a CuAAC reaction with mono-(6-azido-6-deoxy)-β-cyclodextrin (Scheme S4), yielding **1**. The fluorescein-copolymer analog **1′** was prepared by the same synthetic route (Schemes S3 and S5), adding a small amount of fluorescein-*O*-methacrylate in the polymerization step. See the supplemental information for full synthetic procedures and characterization data (Figures S1–S13; Table S2). Toluene was identified as the best solvent to dissolve BMP, CuBr, PMDETA, MPC, and fluorescein *O*-methacrylate for polymerization reactions. As the reaction progresses, the solubility of the growing chain intermediates change and lessen over time, ultimately affecting the molecular weight distribution of the polymer (Tables S1 and S3). Synthesis conditions were optimized to minimize these solubility constraints.

Self-assembly of 1 and 1′ on Ad-functionalized surfaces

Polymer **1** was adsorbed on the **Ti-Ad** or **Glass-Ad** substrates by immersing in a 10 mg/mL aqueous solution of **1** for 12 h. The substrate was then rinsed with deionized water to remove any unconjugated **1** and then allowed to dry under ambient conditions. Surfaces were coated with **1′** by the same method.

Preparation of PMPC-coated AFM tips

PMPC-coated polystyrene microspheres were prepared (Figures S14 and S16) by the grafting polymerization initiated by *tert*-butyl hydroperoxide (TBHP) from the amino group of amine-modified polystyrene microspheres (diameter: 4.0–4.9 μm). The PMPC-coated polystyrene microspheres were glued to the end of a tipless AFM cantilever using ultraviolet curing adhesive. The specific experimental operations are described in detail in supplemental information.

SUPPLEMENTAL INFORMATION

Supplemental information can be found online at https://doi.org/10.1016/j.chempr.2021.11.001.

ACKNOWLEDGMENTS

This work is financially supported by the National Natural Science Foundation of China (52022043); National Key Research and Development Program of China (2018YFB1201902-03); Precision Medicine Foundation, Tsinghua University, China (10001020120); and Capital's Funds for Health Improvement and Research, China (2020-2Z-40810). P.R.M. and Y.S. thank the EPSRC for funding

(EP/V025201/1). A.-J.A. thanks the Royal Society and Global Challenges Research Fund for the award of a Dorothy Hodgkin Fellowship (DHF\R1\180106) and an Enhancement Award (RGF\EA\181065). We thank Dr. Alex Heyman and Dr. Andrew Leech of the University of York NMR Facility and Bioscience Technology Facility, respectively, for their technical support and advice.

AUTHOR CONTRIBUTIONS

Y.W. and Y.S. performed synthesis and characterization of materials. Y.W. carried out microscopy measurements. All authors devised experiments, interpreted data, and prepared the manuscript.

DECLARATION OF INTERESTS

The authors declare no competing interests.

Q7 INCLUSION AND DIVERSITY

One or more of the authors of this paper self-identifies as an underrepresented ethnic minority in science. One or more of the authors of this paper received support from a program designed to increase minority representation in science.

Received: November 28, 2019
Revised: January 10, 2020
Accepted: November 1, 2021
Published: November 24, 2021

REFERENCES

1. Seror, J., Zhu, L., Goldberg, R., Day, A.J., and Klein, J. (2015). Supramolecular synergy in the boundary lubrication of synovial joints. Nat. Commun. *6*, 6497.
2. Lee, S., and Spencer, N.D. (2008). Materials science. Sweet, hairy, soft, and slippery. Science *319*, 575–576.
3. Klein, J. (2013). Hydration lubrication. Friction *1*, 1–23.
4. Ma, L., Gaisinskaya-Kipnis, A., Kampf, N., and Klein, J. (2015). Origins of hydration lubrication. Nat. Commun. *6*, 6060.
5. Jahn, S., Seror, J., and Klein, J. (2016). Lubrication of articular cartilage. Annu. Rev. Biomed. Eng. *18*, 235–258.
6. Maeda, N., Chen, N., Tirrell, M., and Israelachvili, J.N. (2002). Adhesion and friction mechanisms of polymer-on-polymer surfaces. Science *297*, 379–382.
7. Martin, H.J., Schulz, K.H., Bumgardner, J.D., and Walters, K.B. (2007). XPS study on the use of 3-aminopropyltriethoxysilane to bond chitosan to a titanium surface. Langmuir *23*, 6645–6651.
8. Peng, Y., Wang, Z., and Li, C. (2014). Study of nanotribological properties of multilayer graphene by calibrated atomic force microscopy. Nanotechnology *25*, 305701.
9. Yang, H.-K., Khadem, M., Penkov, O.V., and Kim, D.-E. (2019). Increased elasticity and damping capacity of diamond-like carbon coatings by immobilized C60 fullerene clusters. Nanoscale *11*, 2863–2870.
10. Tambe, N.S., and Bhushan, B. (2005). Identifying materials with low friction and adhesion for nanotechnology applications. Appl. Phys. Lett. *86*, 061906.
11. Moro, T., Takatori, Y., Ishihara, K., Konno, T., Takigawa, Y., Matsushita, T., Chung, U.-I., Nakamura, K., and Kawaguchi, H. (2004). Surface grafting of artificial joints with a biocompatible polymer for preventing periprosthetic osteolysis. Nat. Mater. *3*, 829–836.
12. Klein, J. (2009). Chemistry. Repair or replacement—a joint perspective. Science *323*, 47–48.
13. Ishihara, K. (2015). Highly lubricated polymer interfaces for advanced artificial hip joints through biomimetic design. Polym. J. *47*, 585–597.
14. Sorkin, R., Kampf, N., Zhu, L., and Klein, J. (2016). Hydration lubrication and shear-induced self-healing of lipid bilayer boundary lubricants in phosphatidylcholine dispersions. Soft Matter *12*, 2773–2784.
15. Zhulina, E.B., and Rubinstein, M. (2014). Lubrication by polyelectrolyte brushes. Macromolecules *47*, 5825–5838.
16. Yu, J., Jackson, N.E., Xu, X., Morgenstern, Y., Kaufman, Y., Ruths, M., de Pablo, J.J., and Tirrell, M. (2018). Multivalent counterions diminish the lubricity of polyelectrolyte brushes. Science *360*, 1434–1438.
17. Raviv, U., Giasson, S., Kampf, N., Gohy, J.-F., Jérôme, R., and Klein, J. (2003). Lubrication by charged polymers. Nature *425*, 163–165.
18. Li, J., Ueda, E., Paulssen, D., and Levkin, P.A. (2019). Slippery lubricant-infused surfaces: properties and emerging applications. Adv. Funct. Mater. *29*, 1802317.
19. Chen, S., Zhang, N., Zhang, B., Zhang, B., and Song, J. (2018). Multifunctional self-healing ionogels from supramolecular assembly: smart conductive and remarkable lubricating materials. ACS Appl. Mater. Interfaces *10*, 44706–44715.
20. Li, H., Cui, Y., Li, Z., Zhu, Y., and Wang, H. (2018). Fabrication of microcapsules containing dual-functional tung oil and properties suitable for self-healing and self-lubricating coatings. Prog. Org. Coat. *115*, 164–171.
21. Morgese, G., Cavalli, E., Müller, M., Zenobi-Wong, M., and Benetti, E.M. (2017). Nanoassemblies of tissue-reactive, polyoxazoline graft-copolymers restore the lubrication properties of degraded cartilage. ACS Nano *11*, 2794–2804.
22. Irie, T., and Uekama, K. (1997). Pharmaceutical applications of cyclodextrins. III. Toxicological issues and safety evaluation. J. Pharm. Sci. *86*, 147–162.
23. Chiba, J., Sakai, A., Yamada, S., Fujimoto, K., and Inouye, M. (2013). A supramolecular DNA self-assembly based on β-cyclodextrin–adamantane complexation as a bioorthogonal sticky end motif. Chem. Commun. (Camb) *49*, 6454–6456.
24. Rekharsky, M.V., and Inoue, Y. (1998). Complexation thermodynamics of cyclodextrins. Chem. Rev. *98*, 1875–1918.

25. Crini, G. (2014). Review: a history of cyclodextrins. Chem. Rev. *114*, 10940–10975.

26. Liu, Z., Nalluri, S.K.M., and Stoddart, J.F. (2017). Surveying macrocyclic chemistry: from flexible crown ethers to rigid cyclophanes. Chem. Soc. Rev. *46*, 2459–2478.

27. Harada, A., Takashima, Y., and Nakahata, M. (2014). Supramolecular polymeric materials via cyclodextrin–guest interactions. Acc. Chem. Res. *47*, 2128–2140.

28. Yang, X., Yu, H., Wang, L., Tong, R., Akram, M., Chen, Y., and Zhai, X. (2015). Self-healing polymer materials constructed by macrocycle-based host–guest interactions. Soft Matter *11*, 1242–1252.

29. Dai, X., Zhang, Y., Gao, L., Bai, T., Wang, W., Cui, Y., and Liu, W. (2015). A mechanically strong, highly stable, thermoplastic, and self-healable supramolecular polymer hydrogel. Adv. Mater. *27*, 3566–3571.

30. Chen, H., Ma, X., Wu, S., and Tian, H. (2014). A rapidly self-healing supramolecular polymer hydrogel with photostimulated room-temperature phosphorescence responsiveness. Angew. Chem. Int. Ed. Engl. *53*, 14149–14152.

31. Highley, C.B., Rodell, C.B., and Burdick, J.A. (2015). Direct 3D printing of shear-thinning hydrogels into self-healing hydrogels. Adv. Mater. *27*, 5075–5079.

32. de Jong, M.R., Huskens, J., and Reinhoudt, D.N. (2001). Influencing the binding selectivity of self-assembled cyclodextrin monolayers on gold through their architecture. Chemistry *7*, 4164–4170.

33. Mulder, A., Onclin, S., Péter, M., Hoogenboom, J.P., Beijleveld, H., ter Maat, J., García-Parajó, M.F., Ravoo, B.J., Huskens, J., van Hulst, N.F., and Reinhoudt, D.N. (2005). Molecular printboards on silicon oxide: lithographic patterning of cyclodextrin monolayers with multivalent, fluorescent guest molecules. Small *1*, 242–253.

Q9

34. Xu, R., Ma, S., Wu, Y., Zhou, F., and Liu, W. (2018). Promoting lubricity and antifouling properties by supramolecular-recognition-based surface grafting. Langmuir *34*, 13116–13122.

35. Crespo-Biel, O., Péter, M., Bruinink, C.M., Ravoo, B.J., Reinhoudt, D.N., and Huskens, J. (2005). Multivalent host–guest interactions between β-cyclodextrin self-assembled monolayers and poly(isobutene-*alt*-maleic acid)s modified with hydrophobic guest moieties. Chemistry *11*, 2426–2432.

36. Samanta, A., Tesch, M., Keller, U., Klingauf, J., Studer, A., and Ravoo, B.J. (2015). Fabrication of hydrophilic polymer nanocontainers by use of supramolecular templates. J. Am. Chem. Soc. *137*, 1967–1971.

37. Prestch, E., Bühlmann, P., and Badertscher, M. (2009). Structure Determination of Organic Compounds (Springer-Verlag).

38. Moulder, J.F., Stickle, W.F., Sobol, P.E., and Bomben, K.D. (1992). Handbook of X-Ray Photoelectron Spectroscopy (Perkin-Elmer Corp.).

39. Blass, J., Bozna, B.L., Albrecht, M., Krings, J.A., Ravoo, B.J., Wenz, G., and Bennewitz, R. (2015). Switching adhesion and friction by light using photosensitive guest–host interactions. Chem. Commun. (Camb) *51*, 1830–1833.

40. Blass, J., Albrecht, M., Bozna, B.L., Wenz, G., and Bennewitz, R. (2015). Dynamic effects in friction and adhesion through cooperative rupture and formation of supramolecular bonds. Nanoscale *7*, 7674–7681.

41. Guerra, R., Benassi, A., Vanossi, A., Ma, M., and Urbakh, M. (2016). Friction and adhesion mediated by supramolecular host–guest complexes. Phys. Chem. Chem. Phys. *18*, 9248–9254.

42. Wang, Y., Sun, Y., Gu, Y., and Zhang, H. (2019). Articular cartilage-inspired surface functionalization for enhanced lubrication. Adv. Mater. Interfaces *6*, 190180.

43. Vafaeian, B., Adeeb, S., El-Rich, M., Zonoobi, D., Hareendranathan, A.R., and Jaremko, J.L. (2018). Hip joint contact pressure distribution during Pavlik harness treatment of an infant hip: A patient-specific finite element model. J. Biomech. Eng. *140*, 071009.

44. Kyomoto, M., Moro, T., Yamane, S., Watanabe, K., Hashimoto, M., Takatori, Y., Tanaka, S., and Ishihara, K. (2014). Poly(2-methacryloyloxyethyl phosphorylcholine) grafting and vitamin E blending for high wear resistance and oxidative stability of orthopedic bearings. Biomaterials *35*, 6677–6686.

45. Yamane, S., Kyomoto, M., Moro, T., Hashimoto, M., Takatori, Y., Tanaka, S., and Ishihara, K. (2018). Wear resistance of poly(2-methacryloyloxyethyl phosphorylcholine)-grafted carbon fiber reinforced poly(ether ether ketone) liners against metal and ceramic femoral heads. J. Biomed. Mater. Res. B Appl. Biomater. *106*, 1028–1037.

46. Yarimitsu, S., Moro, T., Kyomoto, M., Watanabe, K., Tanaka, S., Ishihara, K., and Murakami, T. (2015). Influences of dehydration and rehydration on the lubrication properties of phospholipid polymer-grafted cross-linked polyethylene. Proc. Inst. Mech. Eng. H *229*, 506–514.

47. Napolitano, S., and Wübbenhorst, M. (2011). The lifetime of the deviations from bulk behaviour in polymers confined at the nanoscale. Nat. Commun. *2*, 260.

48. Fennimore, A.M., Yuzvinsky, T.D., Han, W.-Q., Fuhrer, M.S., Cumings, J., and Zettl, A. (2003). Rotational actuators based on carbon nanotubes. Nature *424*, 408–410.

49. Holmberg, K., and Erdemir, A. (2017). Influence of tribology on global energy consumption, costs and emissions. Friction *5*, 263–284.

50. Perl, A., Gomez-Casado, A., Thompson, D., Dam, H.H., Jonkheijm, P., Reinhoudt, D.N., and Huskens, J. (2011). Gradient-driven motion of multivalent ligand molecules along a surface functionalized with multiple receptors. Nat. Chem. *3*, 317–322.

51. Green, C.P., Lioe, H., Cleveland, J.P., Proksch, R., Mulvaney, P., and Sader, J.E. (2004). Normal and torsional spring constants of atomic force microscope cantilevers. Rev. Sci. Instrum. *75*, 1988–1996.

52. Li, J., Zhang, C., Cheng, P., Chen, X., Wang, W., and Luo, J. (2016). AFM studies on liquid superlubricity between silica surfaces achieved with surfactant micelles. Langmuir *32*, 5593–5599.

53. Varenberg, M., Etsion, I., and Halperin, G. (2003). An improved wedge calibration method for lateral force in atomic force microscopy. Rev. Sci. Instrum. *74*, 3362–3367.

Chem, Volume *8*

Supplemental information

Supramolecular repair of hydration lubrication surfaces

Yixin Wang, Yulong Sun, Alyssa-Jennifer Avestro, Paul R. McGonigal, and Hongyu Zhang

Table of Contents

Supplemental Experimental Procedures

1. Synthetic Procedures for 1 and 1′

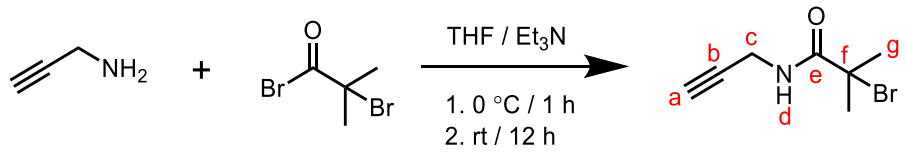

Scheme S1. Synthesis of BMP.

Propargyl 2-bromo-2-methylpropionamide (BMP). Propargylamine (2.40 mL, 35 mmol, 7 eq.) and triethylamine (5.57 mL, 40 mmol, 8 eq.) were dissolved in THF (100 mL) and cooled to 0 °C. A solution of 2-bromopropionyl bromide (5.04 mL, 40 mmol, 8 eq.) in THF (40 mL) was added dropwise and the resulting mixture was stirred at 0 °C for 1 h before allowing to warm to room temperature and stirring for 12 h. Subsequently, the mixture was filtered and the filtrate concentrated by rotary evaporation under reduced pressure. The crude residue was purified by column chromatography (silica gel, petroleum ether/ethanol, 1:1 v/v) to give BMP as a pale yellow solid (2.93 g, 41%), which was characterized by ^{1}H NMR (Supplementary Figure S1), ^{13}C NMR (Supplementary Figure S2) and FTIR spectroscopies (Supplementary Figure S8). **^{1}H NMR** (400 MHz, $CDCl_3$) δ 6.92 (s, 1H, H_d), 4.06 (dd, J = 5.3 Hz, 2.6 Hz, 2H, H_c), 2.28 (t, J = 2.6 Hz, 1H, H_a), 1.97 (s, 6H, H_g). **^{13}C NMR** (100 MHz, $CDCl_3$) δ 171.7 (C_e), 78.9 (C_b), 72.0 (C_a), 62.0 (C_f), 32.4 (C_g), 30.2 (C_c). **IR** ν_{max} 823, 912, 1008, 1060, 1114, 1193, 1268, 1525, 1660, 2119 cm^{-1}.

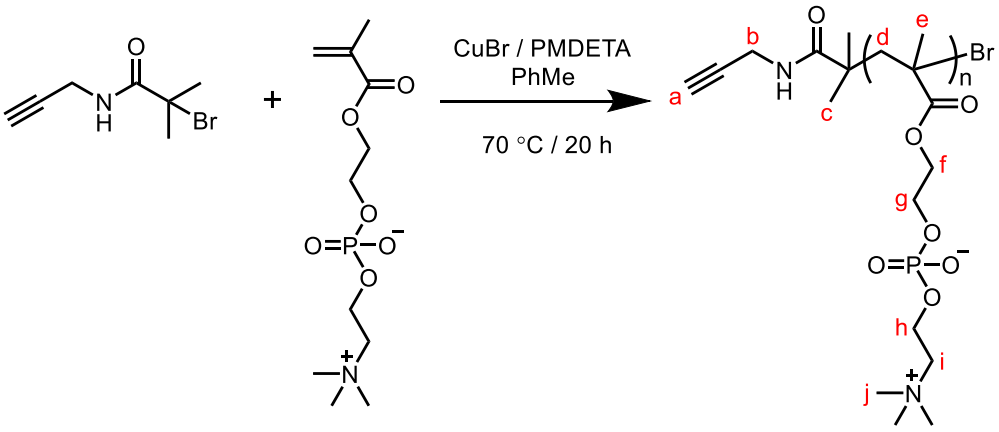

Scheme S2. Synthesis of the alkyne-terminated PMPC.

Alkyne-terminated PMPC. BMP (20 mg, 0.10 mmol, 5 eq.), CuBr (20 mg, 0.14 mmol, 7 eq.), PMDETA (20 mg, 0.12 mmol, 6 eq.) and MPC (400 mg, 1.40 mmol, 70 eq.) were dissolved in anhydrous toluene (10 mL). The mixture was deaerated by applying three cycles of vacuum and backfilling with N_2. The mixture was then heated at 70 °C for 20 h. After cooling, the precipitate was isolated by filtration and dissolved in deionized water (30 mL). The aqueous solution was then dialyzed against fresh deionized water for 48 h to remove unreacted small molecules (molecular weight cut-off: 1 000 Da). The polymer solution was lyophilized, yielding the desired product as a yellow solid (165 mg, 39%), which was characterized by ^{1}H NMR spectroscopy (Supplementary Figure S3), FTIR spectroscopy (Supplementary Figure S8) and gel permeation chromatography (GPC) (water as eluent, the flow rate of the mobile phase: 0.7 mL/min, injection volume: 100 µL, 45 °C). **^{1}H NMR** (400 MHz, D_2O) δ 4.3–4.2 (broad, H_g), 4.2–4.1 (broad, H_h), 4.1–3.9 (m, H_f, H_b), 3.6 (s, H_i), 3.2 (s, H_j) 2.2–1.8 (m, H_a, H_d), 1.2 (t, J = 7.2 Hz, H_c), 1.0–0.8 (broad, H_e). **IR** ν_{max} 792, 966, 1074, 1236, 1483, 1724 cm^{-1}.

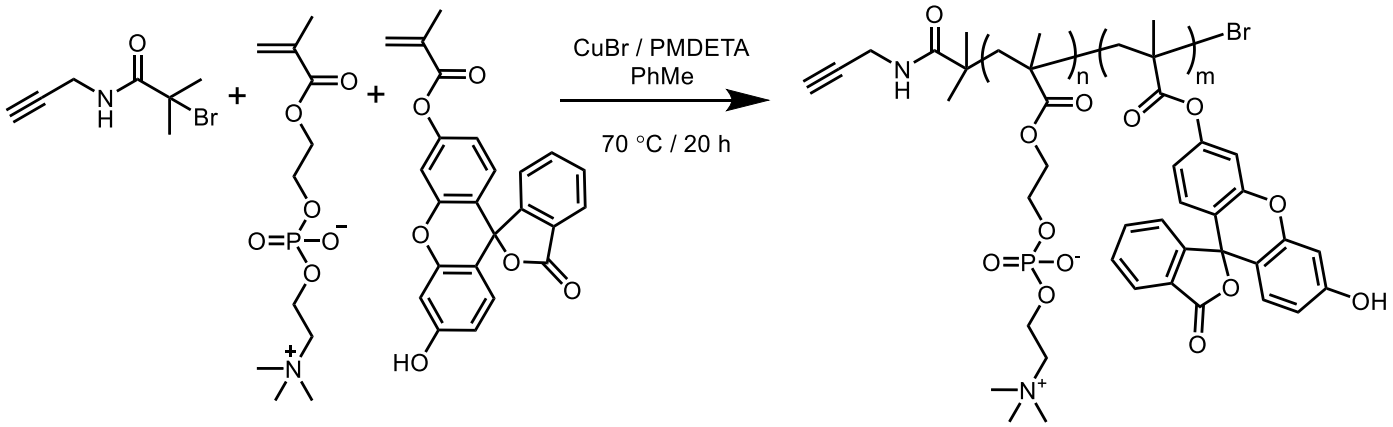

Scheme S3. Synthesis of alkyne-terminated PMPC copolymer with fluorescein *O*-methacrylate.

Fluorophore-labelled alkyne-terminated PMPC. BMP (20 mg, 0.10 mmol, 5 eq.), CuBr (20 mg, 0.14 mmol, 7 eq.), PMDETA (20 mg, 0.12 mmol, 6 eq.), Fluorescein *O*-methacrylate (40 mg, 0.10 mmol, 5 eq.) and MPC (400 mg, 1.40 mmol, 70 eq.) were dissolved in anhydrous toluene (10 mL). The mixture was deaerated by applying three cycles of vacuum and backfilling with N_2. The mixture was then heated at 70 °C for 20 h. After cooling, the precipitate was isolated by filtration and dissolved in deionized water (30 mL). The aqueous solution was then dialyzed against fresh deionized water for 48 h to remove unreacted small molecules (molecular weight cut-off: 1 000 Da). The polymer solution was lyophilized, yielding the desired product as an orange solid (140 mg, 32%), which was characterized by ^{1}H NMR spectroscopy (Supplementary Figure S4), FTIR spectroscopy (Supplementary Figure S8) and GPC (water as eluent, the flow rate of the mobile phase: 0.7 mL/min, injection volume: 100 µL, 45 °C). **^{1}H NMR** (400 MHz, CD_3OD) δ 8.09 – 7.99 (m), 7.79 (t, *J* = 7.9 Hz), 7.72 (t, *J* = 7.8 Hz), 7.32 – 7.15 (m), 6.97 – 6.81 (m), 6.74 – 6.54 (m), 6.35 (s), 5.85 (d, *J* = 2.5 Hz), 5.34 (t, *J* = 4.9 Hz), 4.48 – 3.92 (m), 3.75 (s), 2.19 (t, *J* = 7.6 Hz), 2.04 (dd, *J* = 9.3, 3.7 Hz), 1.68 – 1.54 (m), 1.41 – 1.22 (m), 1.21 – 1.03 (m), 0.90 (t, *J* = 6.7 Hz). **IR** ν_{max} 792, 966, 1074, 1236, 1483, 1724 cm^{-1}.

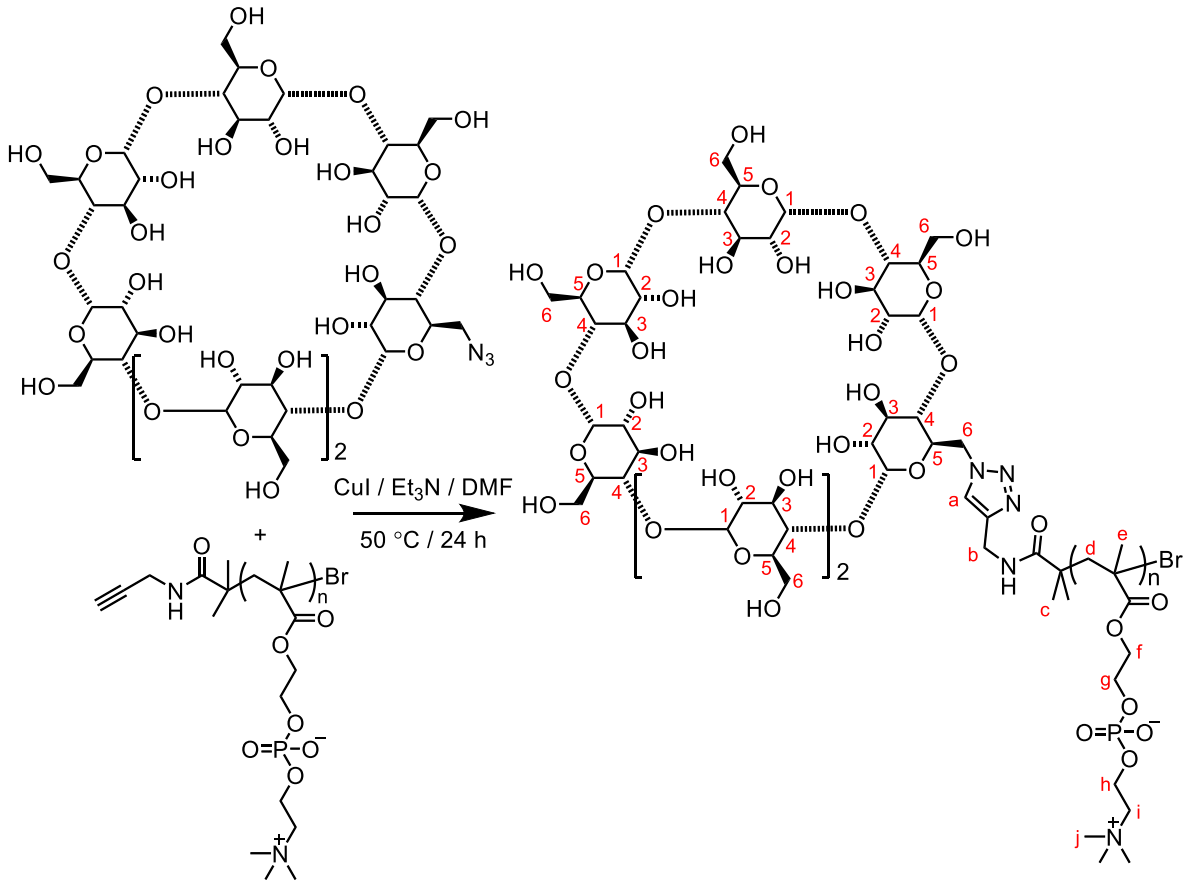

Scheme S4. Synthesis of 1.

1. The alkyne-terminated PMPC (150 mg, 0.024 mmol, 1 eq.), mono-(6-azido-6-deoxy)-β-cyclodextrin (200 mg, 0.17 mmol, 7 eq.), CuI (50 mg), and triethylamine (50 μL) were dissolved in DMF (5 mL). The mixture was heated to reflux under a stream of N_2 gas for 20 min and then maintained under a N_2 atmosphere at 50 °C for 24 h. The reaction mixture was cooled before dialyzing against fresh deionized water for 48 h to remove unreacted small molecules (molecular weight cut-off: 3 500 Da). The green solid product (199 mg, yield: 57%) of **1** was collected after freeze-drying and characterized by ^{1}H NMR spectroscopy (Supplementary Figure S5), FTIR spectroscopy (Supplementary Figure S8) and GPC (water as solvent, the flow rate of the mobile phase: 0.7 mL/min, injection volume: 100 μL, 45 °C). **^{1}H NMR** (400 MHz, D_2O) δ 7.96 (s, H_a), 5.11 (s, H_1), 4.3-4.2 (broad, H_g), 4.2-4.1 (broad, H_h), 4.1-3.9 (broad, H_f), 4.0-3.8 (m, H_3, H_5, H_6), 3.74 (s, H_i), 3.7-3.5 (m, H_2, H_4), 3.3 (s, H_j), 2.0 (broad, H_d), 1.35 (broad, H_c), 0.9 (broad, H_e). **IR** ν_{max} 779, 956, 1064, 1240, 1485, 1722 cm^{-1}.

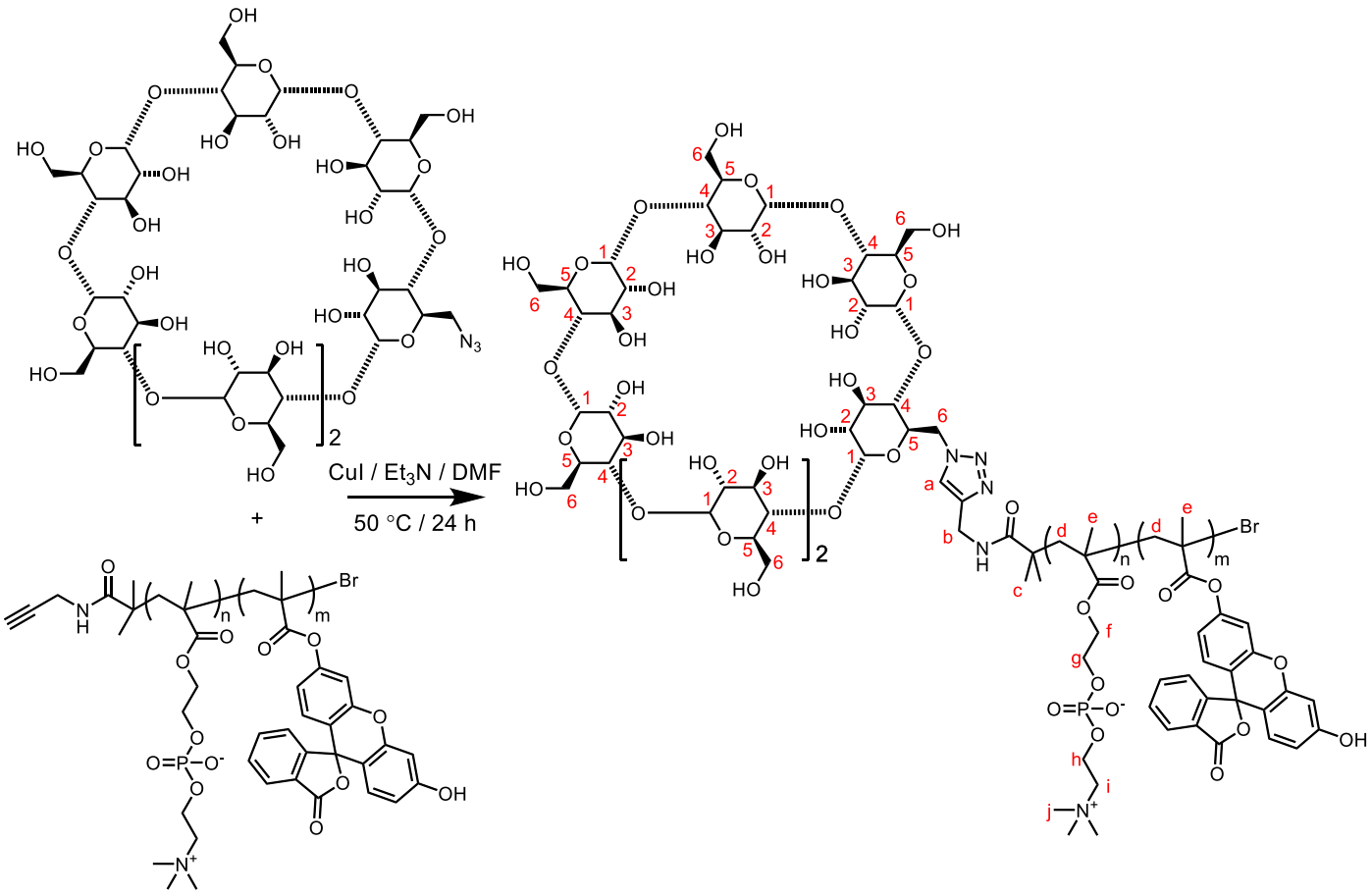

Scheme S5. Synthesis of 1′.

1′. The alkyne-terminated copolymer of MPC and fluorescein *O*-methacrylate (150 mg), mono-(6-azido-6-deoxy)-β-cyclodextrin (200 mg, 0.17 mmol), CuI (50 mg), triethylamine (50 μL) were dissolved in DMF (5 mL). The mixture was heated to reflux under a stream of N_2 gas for 20 min and then maintained under a N_2 atmosphere at 50 °C for 24 h. The reaction mixture was cooled before dialyzing against fresh deionized water for 48 h to remove unreacted small molecules (molecular weight cut-off: 3 500 Da). The orange solid product (185 mg, yield: 53%) of **1′** was collected after freeze-drying and characterized by ^{1}H NMR spectroscopy (Supplementary Figure S6), FTIR spectroscopy (Supplementary Figure S8) and GPC (water as solvent, the flow rate of the mobile phase: 0.7 mL/min, injection volume: 100 μL, 45 °C). **^{1}H NMR** (800 MHz, D_2O) δ 7.46–7.33 (m, H_a & H_{Fl}), 7.07 (s, H_{Fl}), 6.98 (s, H_{Fl}), 6.46 (s, H_{Fl}), 6.37 (s, H_{Fl}), 5.11 (s, H_1), 4.3-4.2 (broad), 4.24–3.18 (m, $H_{f–i}$ & $H_{2–4}$), 3.17–2.79 (m, H_j), 2.0 (broad), 1.92–1.50 (broad, H_d), 1.36 (s, H_c), 0.92–0.50 (m, H_e). Peaks arising from the fluorescein moiety are labelled H_{Fl}. **IR** ν_{max} 779, 956, 1064, 1240, 1485, 1722 cm^{-1}.

2. NMR Spectroscopic Characterizaton

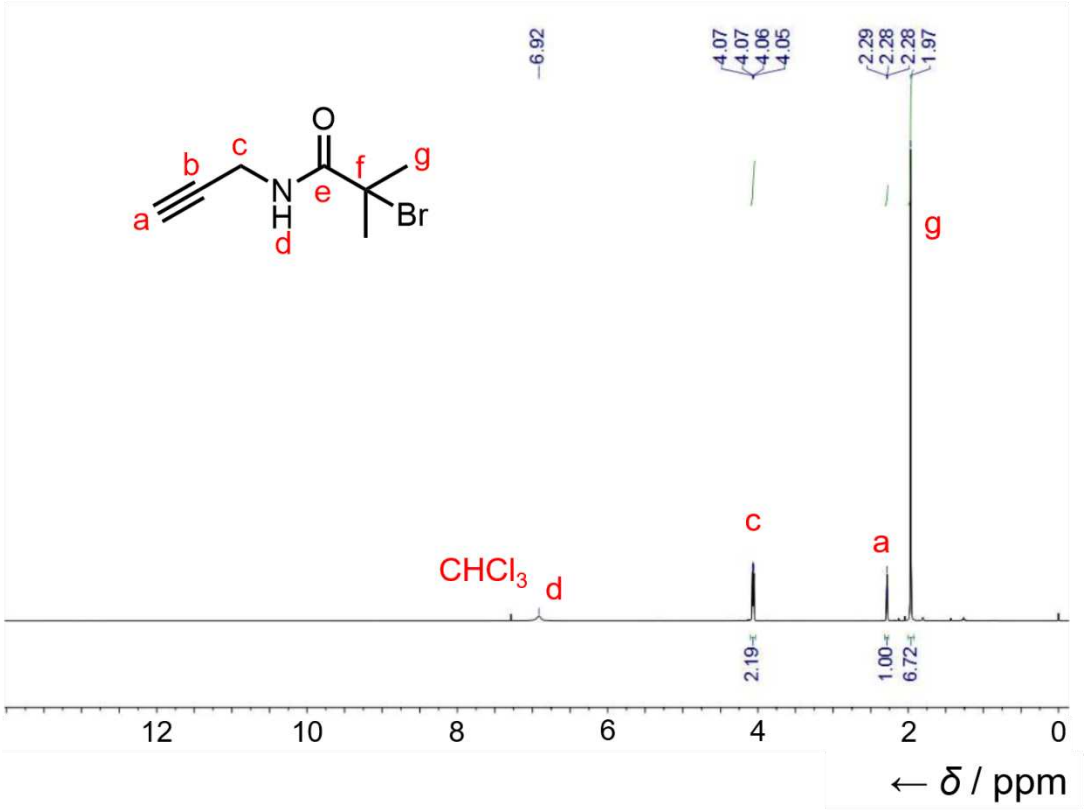

Figure S1. ^{1}H NMR spectrum of BMP ($CDCl_3$, 25 °C, 400 MHz).

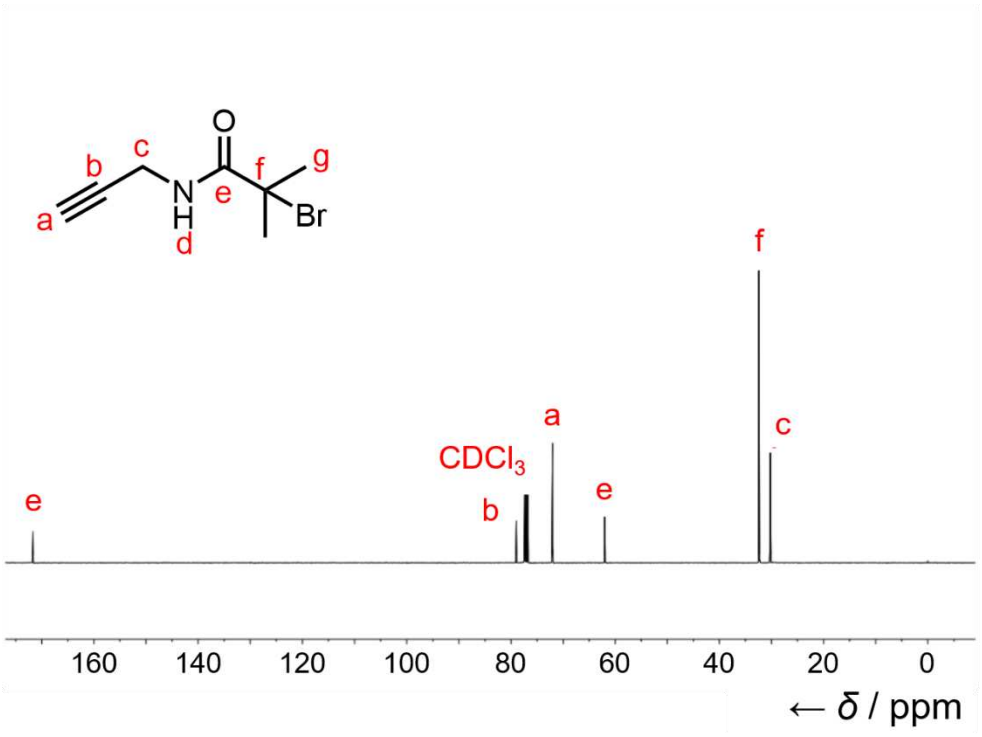

Figure S2. ^{13}C NMR spectrum of BMP ($CDCl_3$, 25 °C, 100 MHz).

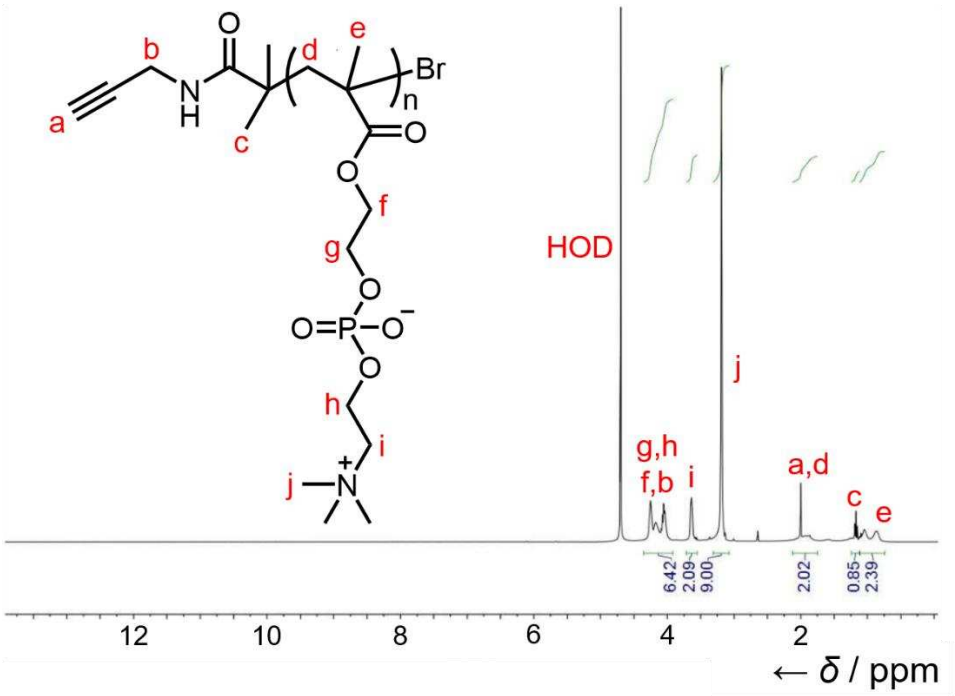

Figure S3. ^{1}H NMR spectrum of the alkyne-terminated PMPC (D_2O, 25 °C, 400 MHz).

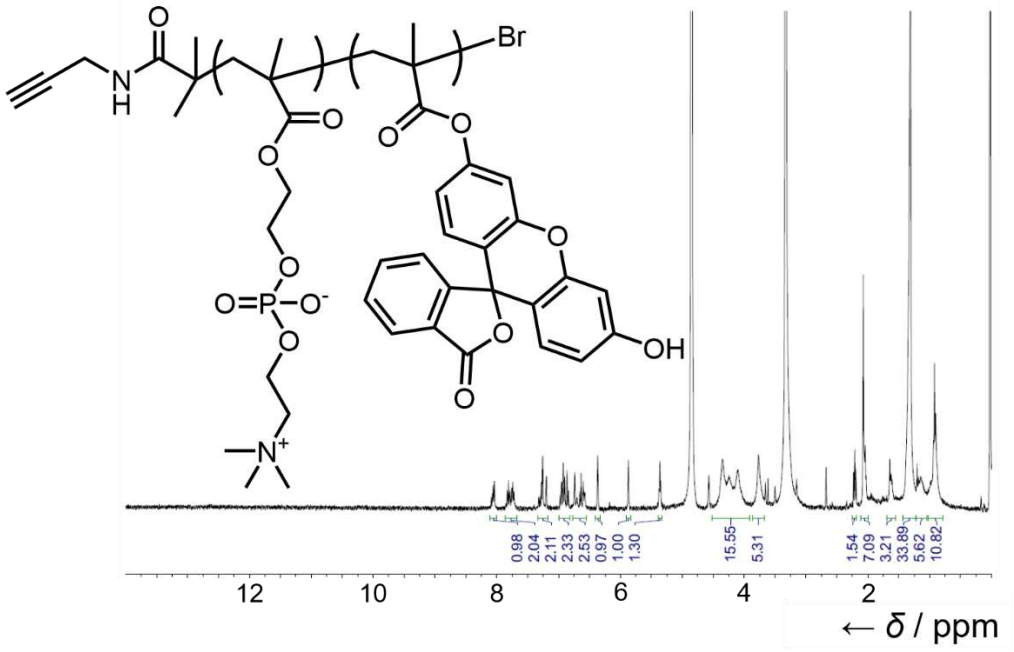

Figure S4. ^{1}H NMR spectrum of fluorescein-labelled alkyne-terminated PMPC (CD_3OD, 25 °C, 400 MHz).

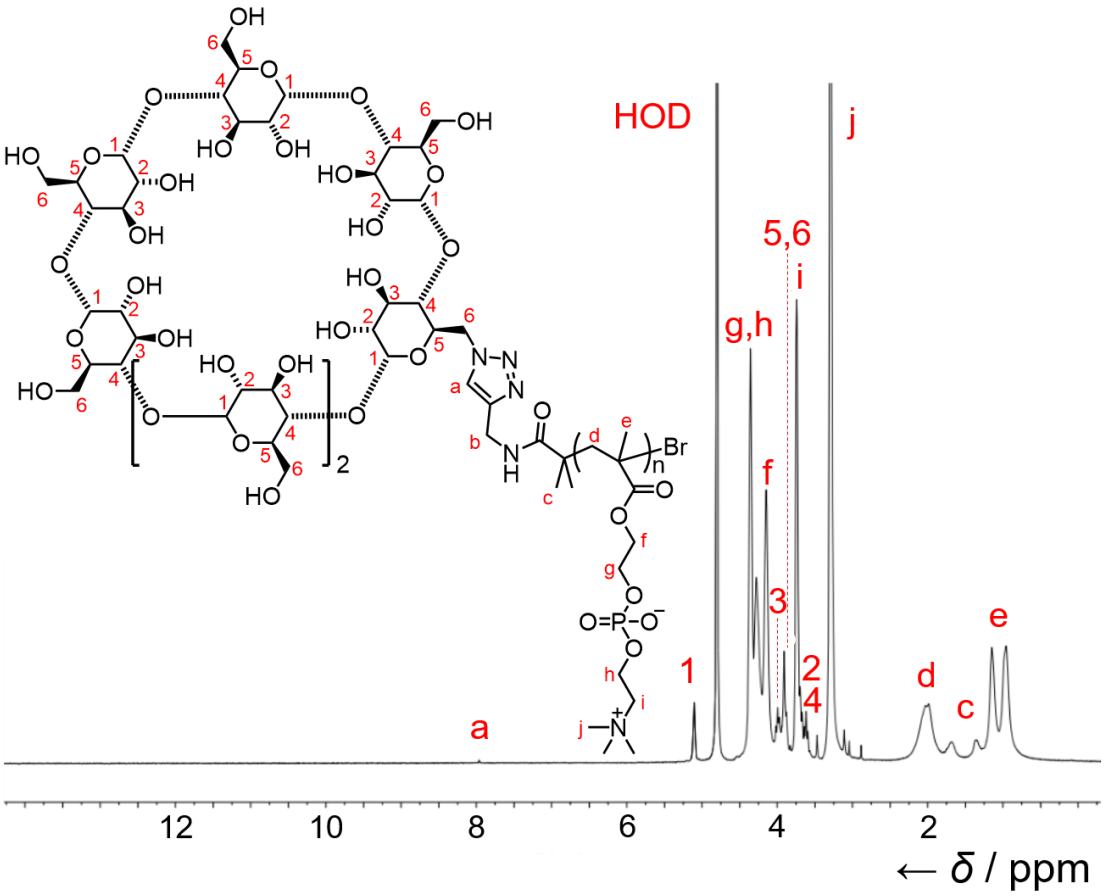

Figure S5. ^{1}H NMR spectrum of 1 (D_2O, 25 ℃, 400 MHz).

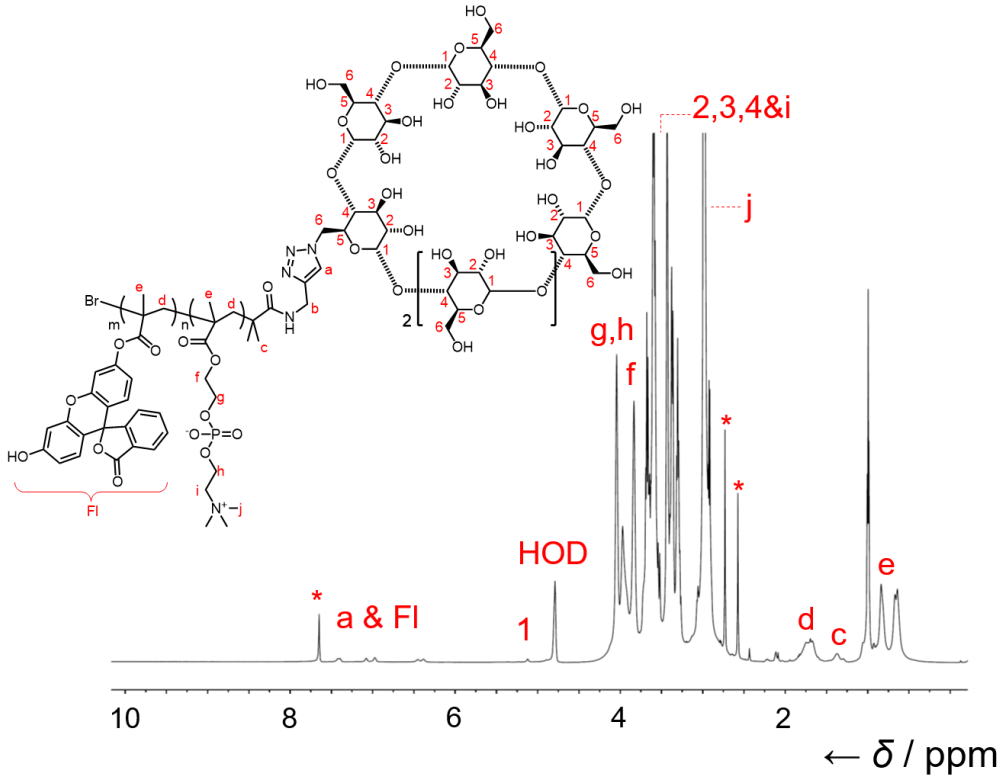

Figure S6. ^{1}H NMR spectrum of 1′ (D_2O, 25 °C, 800 MHz), * indicates residual *N*,*N*-dimethylformamide peaks.

2.1. DOSY NMR Analysis

Diffusion-ordered NMR spectroscopy (DOSY) experiments were performed Figures S7–8) in an attempt to estimate the average molecular weight of PMPC-derived polymers used in this study. Measurements were carried out using a Bruker AVIII HD500 spectrometer. Assuming these molecules adopt a spherical structure in D_2O, the molar hydrodynamic radius (r_H) can be determined using the Stokes–Einstein equation:

$$r_H = \frac{k_B T}{6\pi\eta D}$$

where k_B is the Boltzmann constant (1.3801×10^{-23} J·K^{-1}), T the temperature (293 K), η the solvent viscosity (1.25×10^{-3} Pa·s for D_2O at 293 K) and D the diffusion coefficient or rate (m^2·s^{-1}), as determined by experiment. The value of r_H is then used to estimate (Table S1) the weight average molar mass (M_w) based on the following relationship:

$$M_w = \frac{4\pi {r_H}^3 \rho N}{3}$$

where ρ is the solvent density (1.00 g·cm^{-3}) and N is the Avogadro constant (6.022×10^{23} g·mol^{-1}).

Table S1. Estimated weight average molar masses of 1 and 1′ measured by DOSY NMR.

Polymer	D / 10^{-11} m^2·s^{-1}	r_H / nm	$M_{w(DOSY)}$ / kDa
1	2.87	6.0	540
1′	4.57	3.8	134

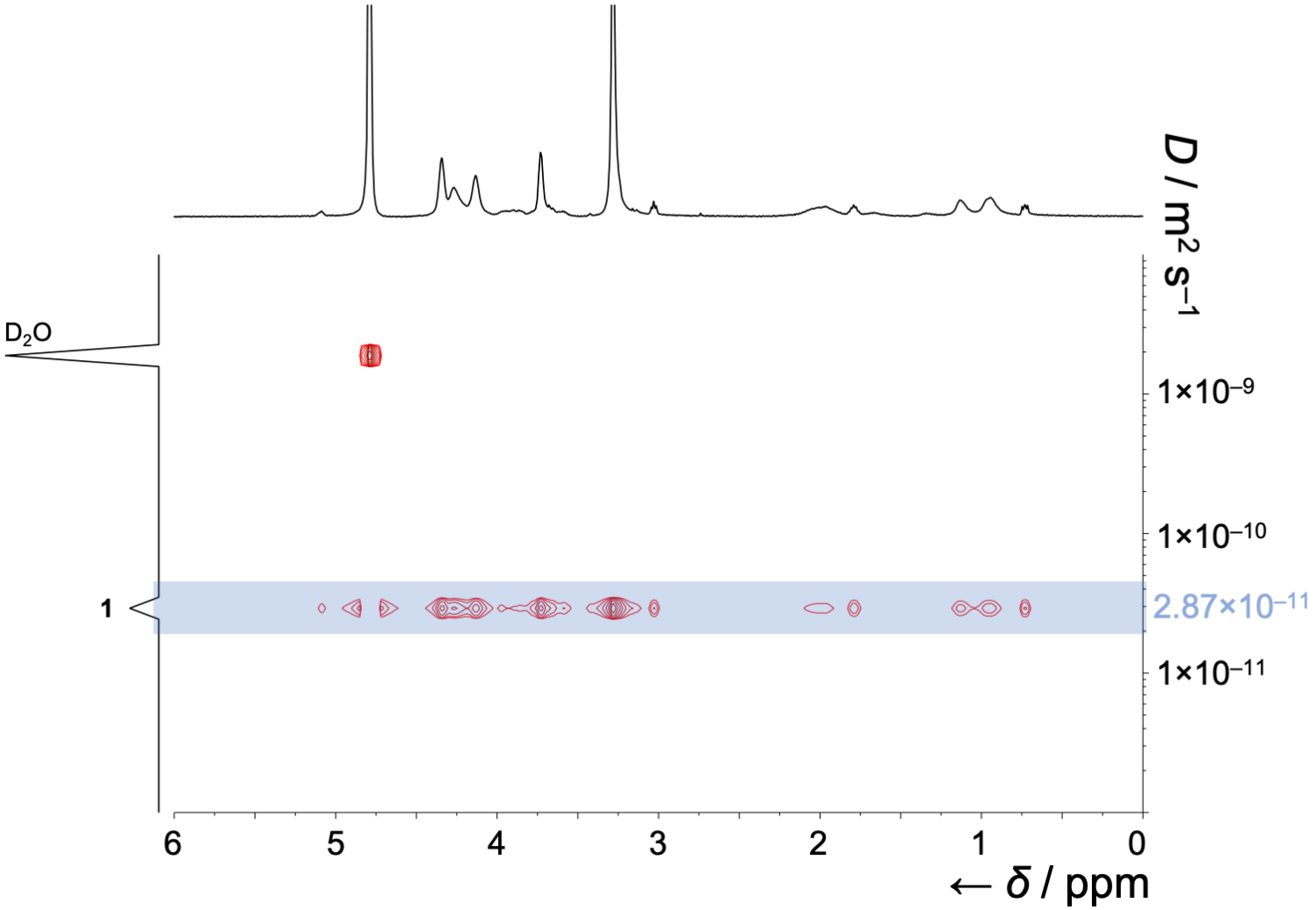

Figure S7. Diffusion-ordered NMR spectrum of 1 (D_2O, 20 ºC, 500 MHz). A diffusion coefficient of 2.87×10^{-11} $m^2\cdot s^{-1}$ was measured for the major sample component, which gives a molar hydrodynamic radius of 6.0 nm and an *estimated* M_w of ca. 540 kDa for **1**.

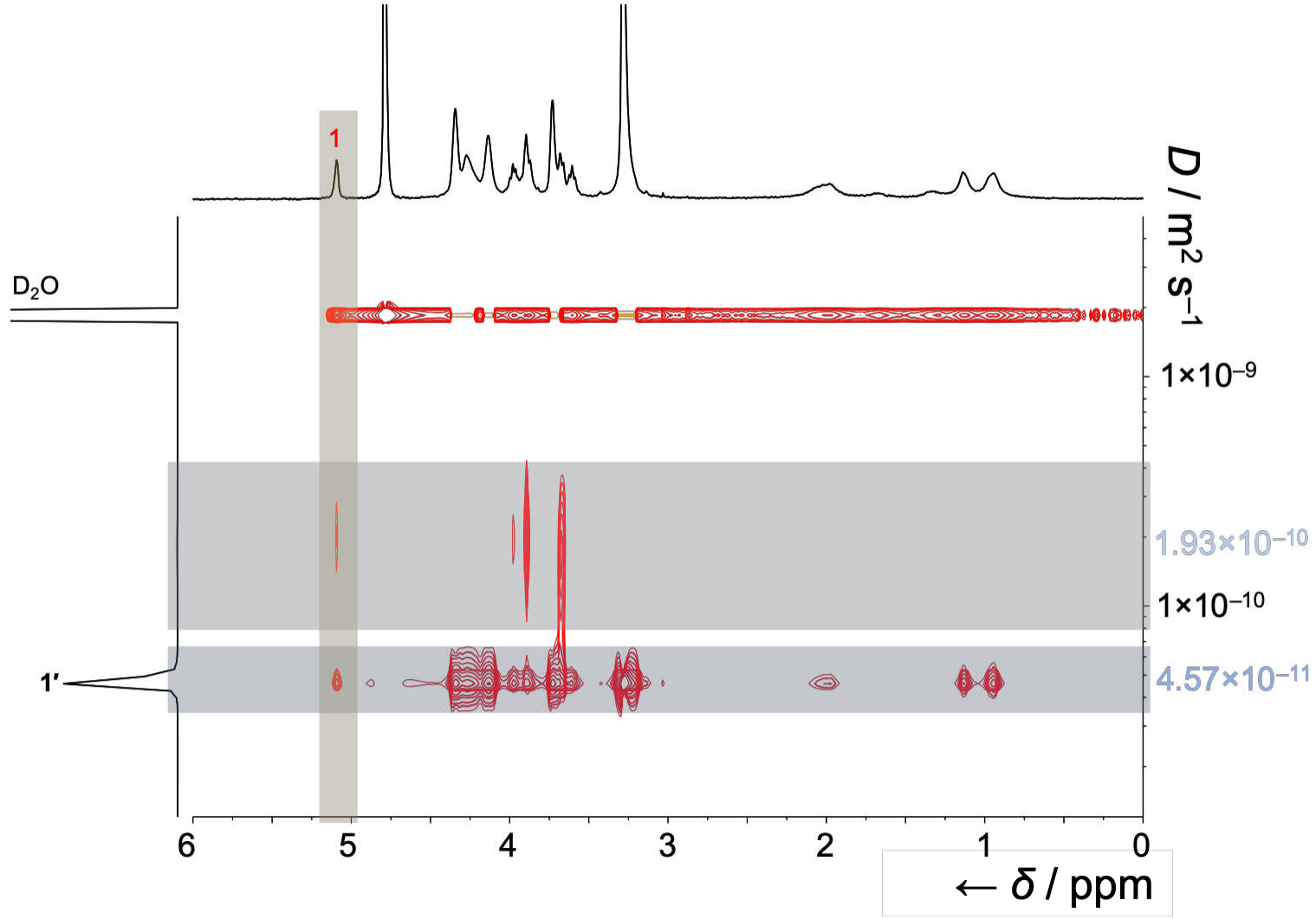

Figure S8. Diffusion-ordered NMR spectrum of 1′ (D_2O, 20 ºC, 500 MHz). A diffusion coefficient of 4.57×10^{-11} $m^2\cdot s^{-1}$ was measured for the major sample component, which gives a molar hydrodynamic radius of 3.8 nm and an *estimated* M_w of ca. 134 kDa for **1′**. In this sample, a smaller fast-diffusing species (D = 1.93×10^{-10} $m^2\cdot s^{-1}$) is also observed at low intensity, which we tentatively attribute to trace unreacted β-CD on account of the shared chemical shift at δ 5.09 ppm corresponding to H_1 of the pyranose ring (c.f. Figure S6 labelling).

3. FTIR Spectroscopy

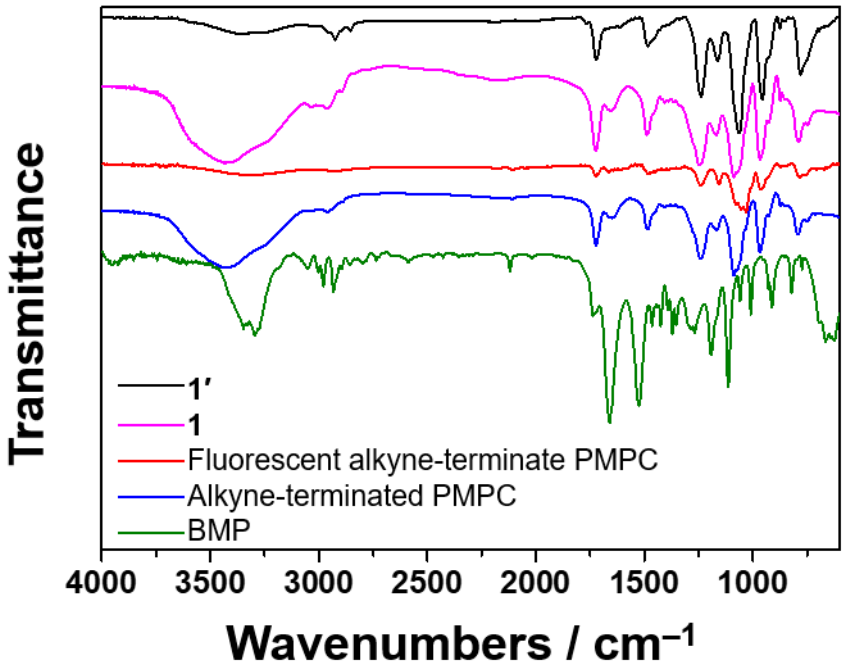

Figure S9. FTIR spectra of the synthesized compounds. The data are consistent with successful CuAAC reaction between the alkynyl-terminated PMPC derivatives and mono-6-azido-deoxy-β-CD as the characteristic alkyne peak at 2119 cm^{-1} is absent after the reaction.

4. Fluorescence Spectroscopy

The proportion of fluorescein contained in the copolymers was measured by comparing their fluorescence spectra (Figure S10) to a fluorescein *O*-methacrylate standard (Figure S10). Three-dimensional (3D) fluorescence measurements were performed using a F-7000 Fluorescence Spectrophtotmeter, Hitachi, Japan. Fluorescein emission is expected in the region of 500–550 nm when excited with 400–500 nm light. The alkyne-terminated PMPC and **1**, which both lack fluorescein, show no emission in this area of 3D fluorescence spectra. A fluorescein peak is observed, however, for the fluorescein-labelled alkyne-terminated PMPC and **1′** copolymers, confirming successful copolymerization and fluorescent labelling.

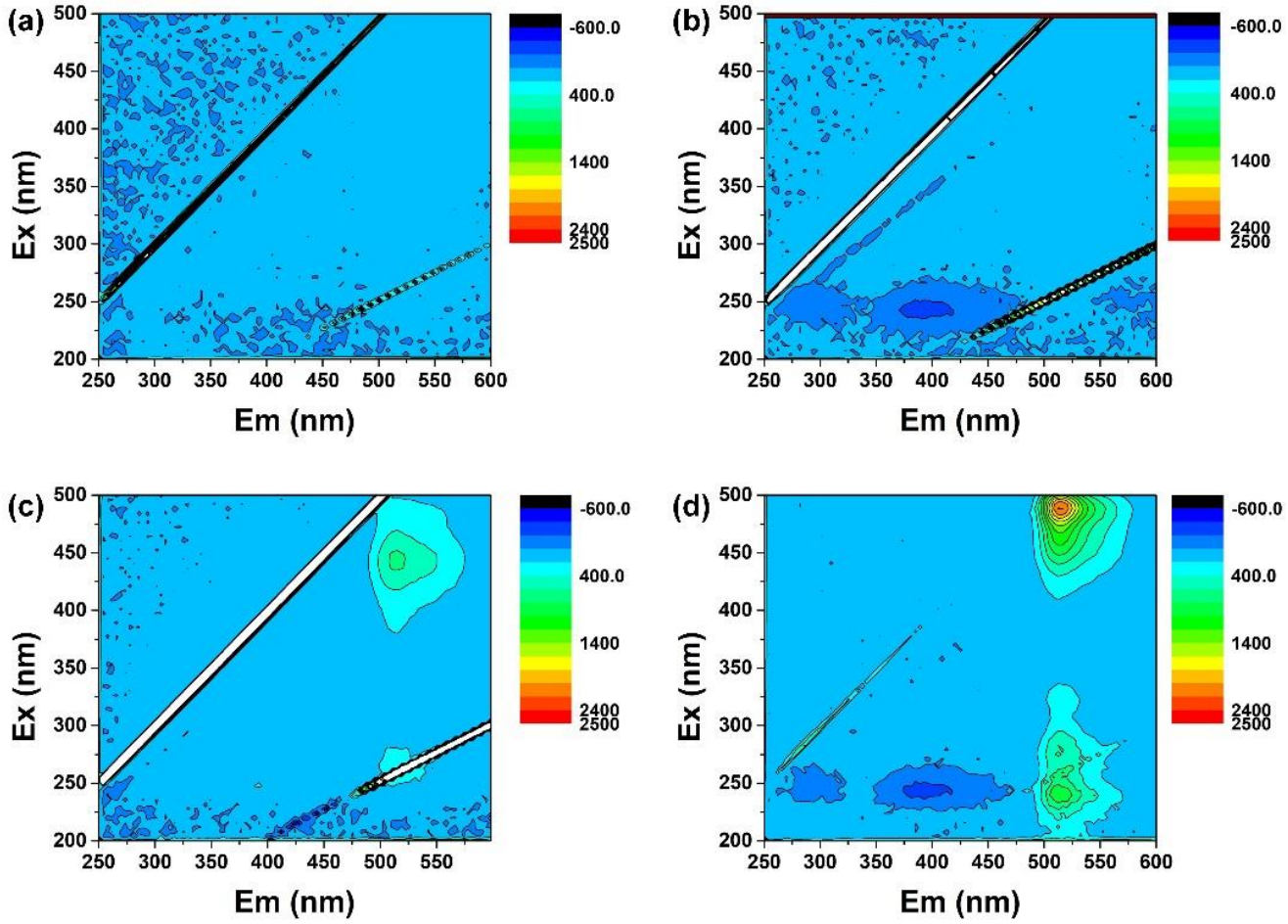

Figure S10. 3D Fluorescence spectra of (a) alkyne-terminated PMPC, (b) 1, (c) fluorescein-labelled alkyne-terminated PMPC and (d) 1′ aqueous solutions.

To quantify the proportion of fluorescein monomers incorporated in **1′**, the peak intensities were compared to a standard curve (Figure S11) established using known concentrations of fluorescein *O*-methacrylate.

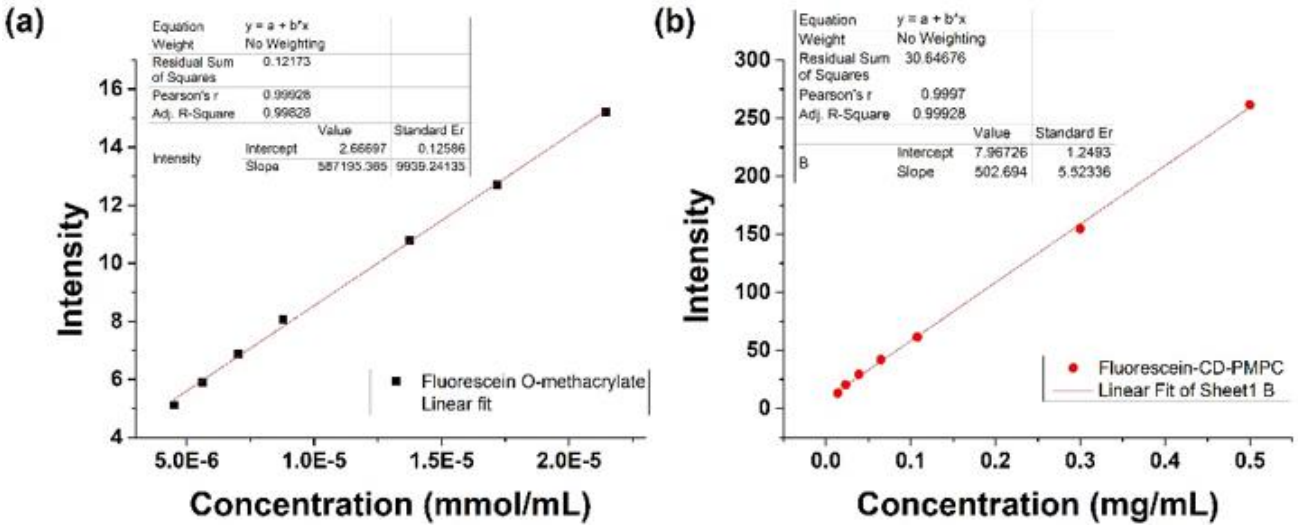

Figure S11. Standard curve fitting of methanolic solutions of (a) fluorescein *O*-methacrylate and (b) 1′. λ_{ex} = 485 nm, λ_{em} = 516 nm.

In the concentration ranges studied, the fluorescence intensities varied linearly with changes in concentration, allowing us to calculate (Table S2) the effective concentration of fluorescein monomers in solutions of **1′**. The average fluorescein content in **1′** is 1.07 μmol/mg.

Table S2. Calculated fluorescein content of 1′ solutions.

Concentration (mg/mL)	Intensity	Fluorescein content ($\times 10^{-5}$ mmol/mL)	Fluorescein per unit mass of **1′** (μmol/mg)
0.5	261.5	44.1	0.882
0.3	154.8	25.9	0.864
0.108	61.61	10.0	0.930
0.0648	42.19	6.73	1.04
0.03888	29.34	4.54	1.17
0.02333	20.41	3.02	1.30
0.014	13.25	1.80	1.29

5. XPS Characterization of 1

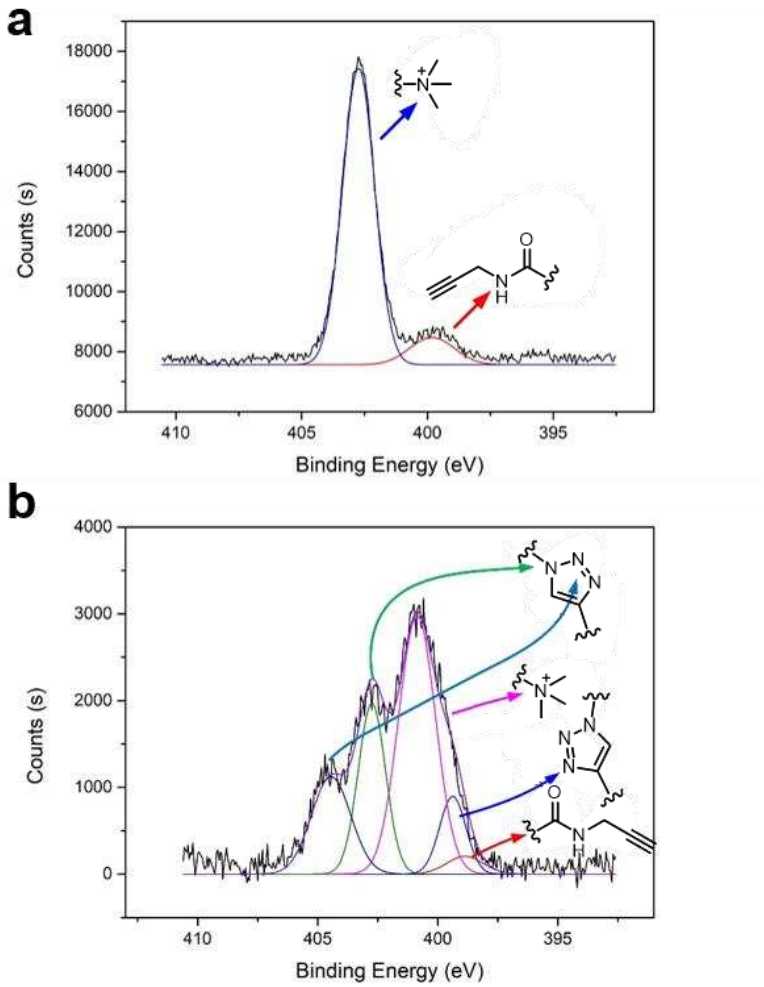

Figure S12. XPS spectra of (a) the alkyne-terminated PMPC and (b) the polymer 1 isolated from a CuAAC reaction. Peak-fitting traces are overlaid, showing an increase in the number of N signals resulting from successful triazole formation.

6. Size Exclusion Chromatography

Size-exclusion chromatography with multi-angle laser light scattering (SEC-MALLS) experiments were conducted (Figure S13) on a system comprising a Wyatt HELEOS-II multi-angle light scattering detector and a Wyatt rEX refractive index detector linked to a Shimadzu HPLC system (SPD-20A UV detector, LC20-AD isocratic pump system, DGU-20A3 degasser and SIL-20A autosampler). Work was conducted at room temperature (20 ± 2 °C). The running solvent (0.2 M sodium nitrate prepared using high-purity water) was passed through a 0.2 μm filter before use, with a further 0.1 μm filter present in the flow path. The column was equilibrated with at least two column volumes of solvent before use and flow was continued at the working flow rate until baselines for UV, light scattering and refractive index detectors were all stable. Molar masses are estimated based on refractive index and light scattering data, where a value of 0.19 mL/g was used as an estimate for refractive index increment (dn/dc).

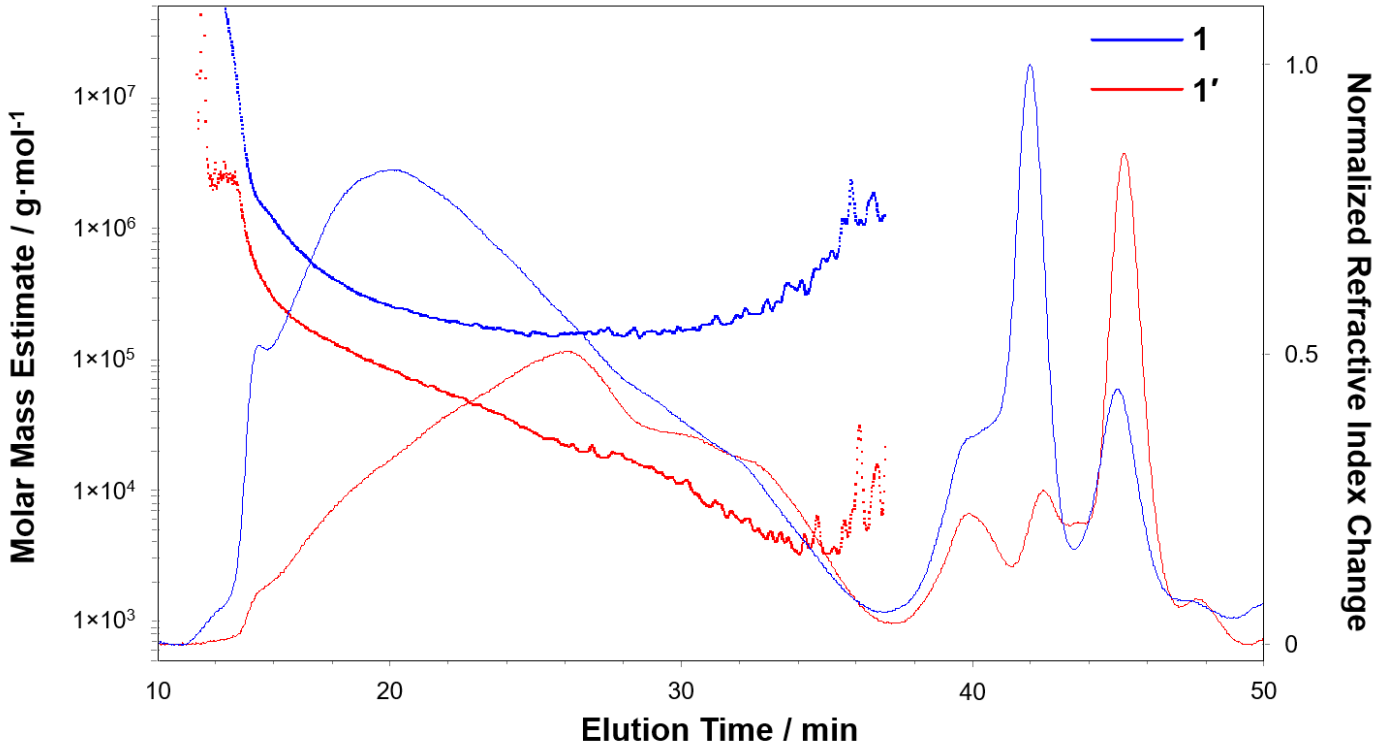

Figure S13. SEC-MALLS refractive index chromatograms (solid lines) and estimated M_w (dotted lines) for polymers 1 and 1′.

Quantification of the polymer molar masses and polydispersities was complicated by the lack of chromophores in **1** for UV-vis absorbance monitoring, the tendency of **1** to aggregate in aqueous solutions, and apparent association of **1** and **1′** with the column matrix. The bed volume of the column is reached at approximately 43 min (22.5 mL), so the appearance of peaks eluting after this time is indicative of adsorption effects, i.e., some of the sample associating with the column matrix, which is Superdex (a cross-linked carbohydrate material). For this reason, no molar mass estimation is made for the additional signals appearing after the major, broad peak ends at about 38 min.

Polymers **1** and **1′** each give a significant refractive index response over a broad peak area, suggesting that both are polydisperse. As there are no obviously resolved peaks, areas (“peak regions”) for analysis were set on an arbitrary basis as follows: (1) 15.8 to 28 min, the early part of the fractionation range; (2) 28 to 32 min, the middle part; (3) 32 to 37 min, the later part; and (4) 37 to 40.5 min, the small moleules. The estimated weight average molar masses (M_w) and polydispersities (PDI) for the polymers in these peak regions, as well as the weight fraction of the eluted material that they correspond to (wt frac.), are given in Table S3.

Table S3. Estimated weight average molar masses and PDIs of 1 and 1′ measured by SEC-MALLS. The highlighted row shows the values for the peak region containing the majority of the polymer.

Peak Region	Elution Time / min		1			1′		
	From	To	$M_{w(SEC)}$[a] kDa	PDI	wt frac.	$M_{w(SEC)}$[a] kDa	PDI	wt frac.
1	15.8	28.0	**297**	**1.32**	**0.73**	**59.1**	**1.62**	**0.61**
2	28.0	32.0	173	1.01	0.14	11.5	1.11	0.20
3	32.0	37.0	469	1.42	0.07	5.1	1.12	0.13
4	37.0	40.5	477	1.95	0.06	3.9	1.79	0.06

[a] M_w estimations are based on an assumed refractive index increment of 0.19. It is notable that the M_W estimates are higher close to the void volume but do not tail off rapidly, which is likely a result a rather 'sticky' high-M_W material eluting slowly from the column. The large particles dominate the light-scattering signal, thus resulting in over-estimation of M_W.

7. AFM Tip Functionalization

Preparation of PMPC-Coated AFM Colloidal Tips

A 0.5 mL aqueous suspension of 25 mg amine-modified polystyrene microspheres (4.0-4.9 μm) was added to an aqueous solution of MPC (50 mM, 30 mL), before adding 100 μL of *tert*-butyl hydroperoxide (TBHP). The reaction mixture was heated at 80 °C for 12 h under a N_2 atmosphere, after which the PMPC-coated microspheres was collected by centrifugation and dried under vacuum. The average diameter of the PMPC-coated microsphere was measured by dynamic light scattering (DLS), as shown in Figure S14. The PMPC-coated microspheres was glued on the jut of the AFM cantilever using ultraviolet-cured adhesive, irradiating with UV-light for 40 min.

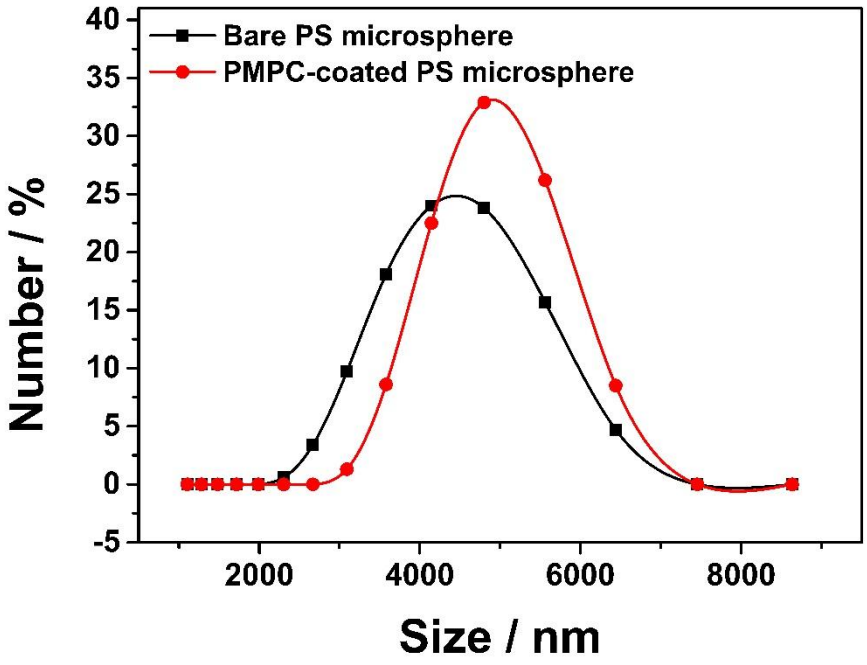

Figure S14. The diameters of polystyrene microspheres before and after PMPC coating

The diameters of polystyrene microspheres before and after PMPC coating was measured by DLS, using 1 mg/mL aqueous suspensions. The average diameter of a PMPC-coated microsphere is 5.314 μm while the average diameter of a bare polystyrene microsphere is 4.916 μm.

Preparation of β-CD-Coated AFM Colloidal Tip

A 0.5 mL aqueous suspension of 25 mg amine-modified polystyrene microspheres (4.0-4.9 μm) was added to a solution of mono-6-*O*-(*p*-toluenesulfonyl)- β-cyclodextrin in acetonitrile (100 mM, 30 mL). The reaction vessel was sealed with a septum and heated to 50 °C for 12 h, after which the β-CD coated microspheres were collected by centrifugation and washed with water four times. The microspheres were then dried under vaccum. The average diameter of the β-CD-coated microspheres was measured by DLS, as shown in Figure S15. The β-CD coated microsphere was glued on the jut of the AFM cantilever using ultraviolet curing adhesive and followed by curing under UV-light for 40 min.

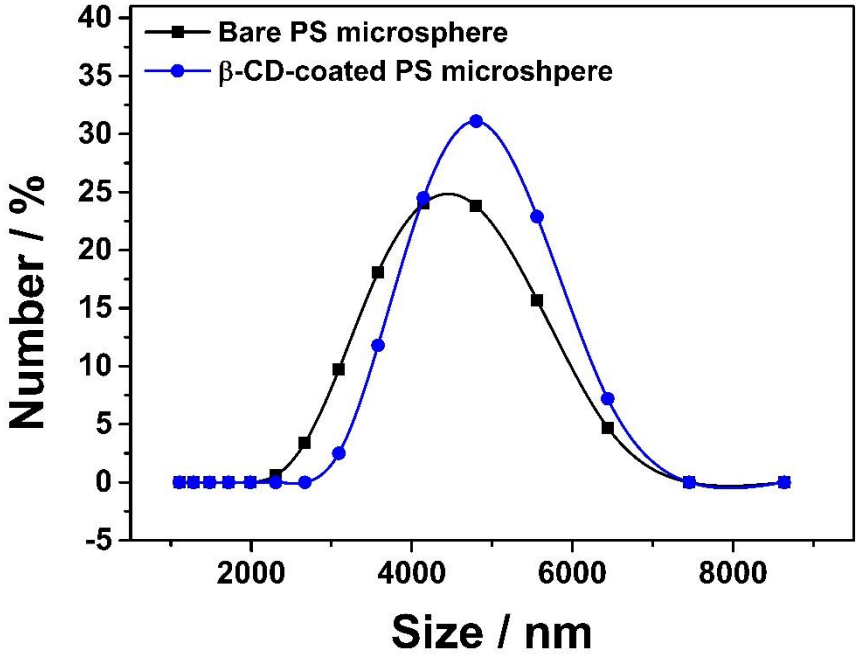

Figure S15. The diameters of polystyrene microspheres before and after β-CD coating.

The diameters of polystyrene microspheres before and after β-CD coating was measured by DLS, using 1 mg/mL aqueous suspensions. The average diameter of a β-CD-coated microsphere is 5.032 μm while the average diameter of a bare polystyrene microsphere is 4.916 μm.

7.1 Calculation of AFM Contact Area

According to Hertz contact theory,[S1] the radius of the contact area is calculated as:

$$a = \sqrt[3]{\frac{3}{4} R_0 (\frac{1-{\nu_1}^2}{E_1} + \frac{1-{\nu_2}^2}{E_2}) \mathrm{P}}$$

where R_0 is the radius of the microsphere glued on the AFM colloidal tip, P is the normal force applied to the surface, E_1 and E_2 are the Young's moduli of polystyrene and glass, respectively, ν_1 and ν_2 are Poisson's ratios of polystyrene and glass, respectively.

Taking the R_0 as 2.5 μm, P as 400 nN, E_1 as 3.2 GPa, E_2 as 72 GPa, ν_1 as 0.38, and ν_2 0.22,[S2] we calculate the theoretical radius of the contact area between an AFM colloidal tip and glass to be 59.48 nm.

7.2 Calculation of Pressure in AFM Contact Area

We calculated the maximal pressure in the contact area between an AFM colloidal tip and Ti-6Al-4V wafer according to Hertz contact theory.[S1] The maximal pressure q_0 in the contact area is calculated as:

$$q_0 = \sqrt[3]{\frac{6}{\pi^3} \cdot \frac{1}{{R_0}^2} \cdot \frac{P}{(\frac{1-{\nu_1}^2}{E_1} + \frac{1-{\nu_2}^2}{E_2})^2}}$$

where R_0 is the radius of the microsphere glued on the AFM colloidal tip, P is the normal force applied to the surface, E_1 and E_2 are the Young's moduli of polystyrene and Ti-6Al-4V, respectively, ν_1 and ν_2 are Poisson's ratios of polystyrene and Ti-6Al-4V, respectively.

Taking the R_0 as 2.5 μm, P as 400 nN, E_1 as 3.2 GPa, E_2 as 114 GPa, ν_1 as 0.38, and ν_2 0.28,[S2] we calculate the theoretical pressure in the contact area between an AFM colloidal tip and Ti-6Al-4V wafer to be 54.65 MPa, which exceeds the actual contact pressure in natural hip joint.[S3]

7.3 Scanning Electron Microscope (SEM) Image of AFM Tip

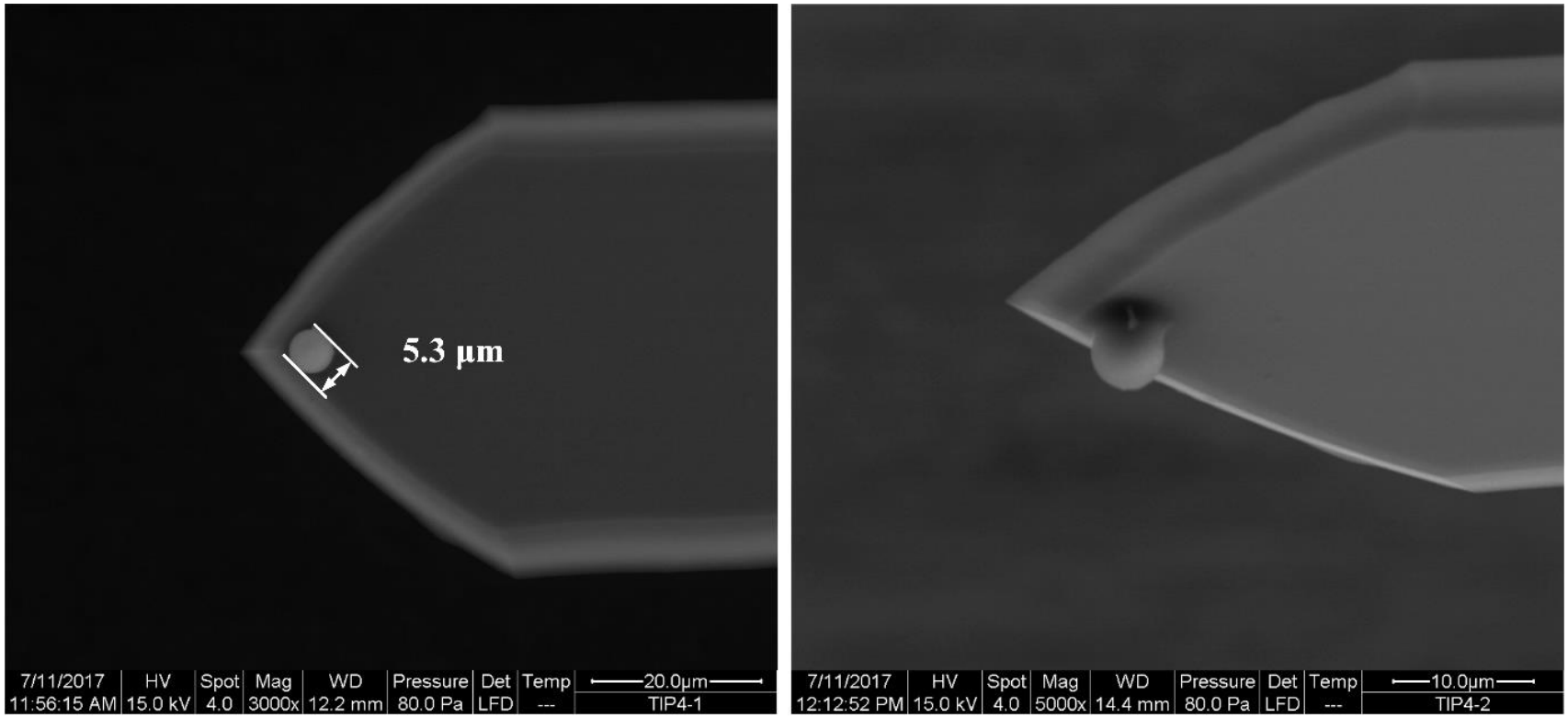

Figure S16. SEM images of PMPC-coated colloidal AFM tip.

8. Preparation of Ad-Coated Ti Alloy Wafers

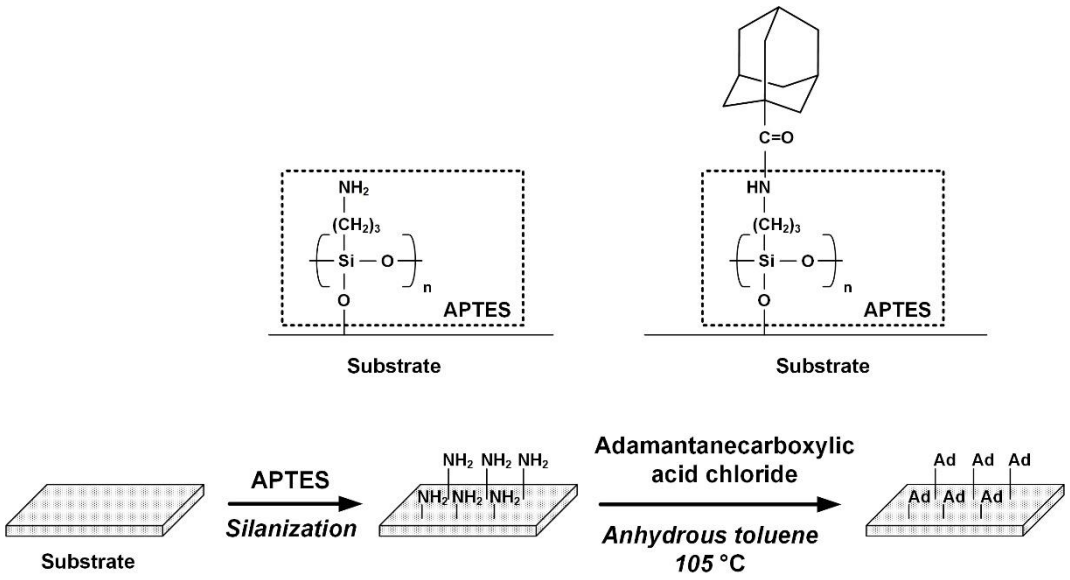

Scheme S6. Schematic representation of the Ad coating on Ti alloy wafers.

The surfaces of commercially sourced Ti-6Al-4V wafers were firstly cleaned by ultrasonication in pure water and acetone for 5 min each and dried in N_2 flow. The amination of the wafers was performed by adding 100 μL of aminopropyltriethoxysilane (APTES) solution (72% ethanol, 8% water, 20% APTES, v/v/v) onto the wafers at room temperature. After 12 h, the wafers were immersed in ultrapure water and subjected to ultrasonication to remove the unconnected materials. The wafers were immersed in anhydrous toluene solution of 1-adamantanecarboxylic acid chloride (1 mmol/L, 100 mL) and then refluxed under a N_2 atmosphere at 115 °C for 12 h. The as-made wafers were washed by sonicating while immersed in pure water to remove unreacted molecules, before removing the wafers from solution and blowing with N_2 to dry. The coated wafers were charaterised by ATR-FTIR analysis and XPS spectra.

9. XPS Spectra of Functionalized Glass Slides

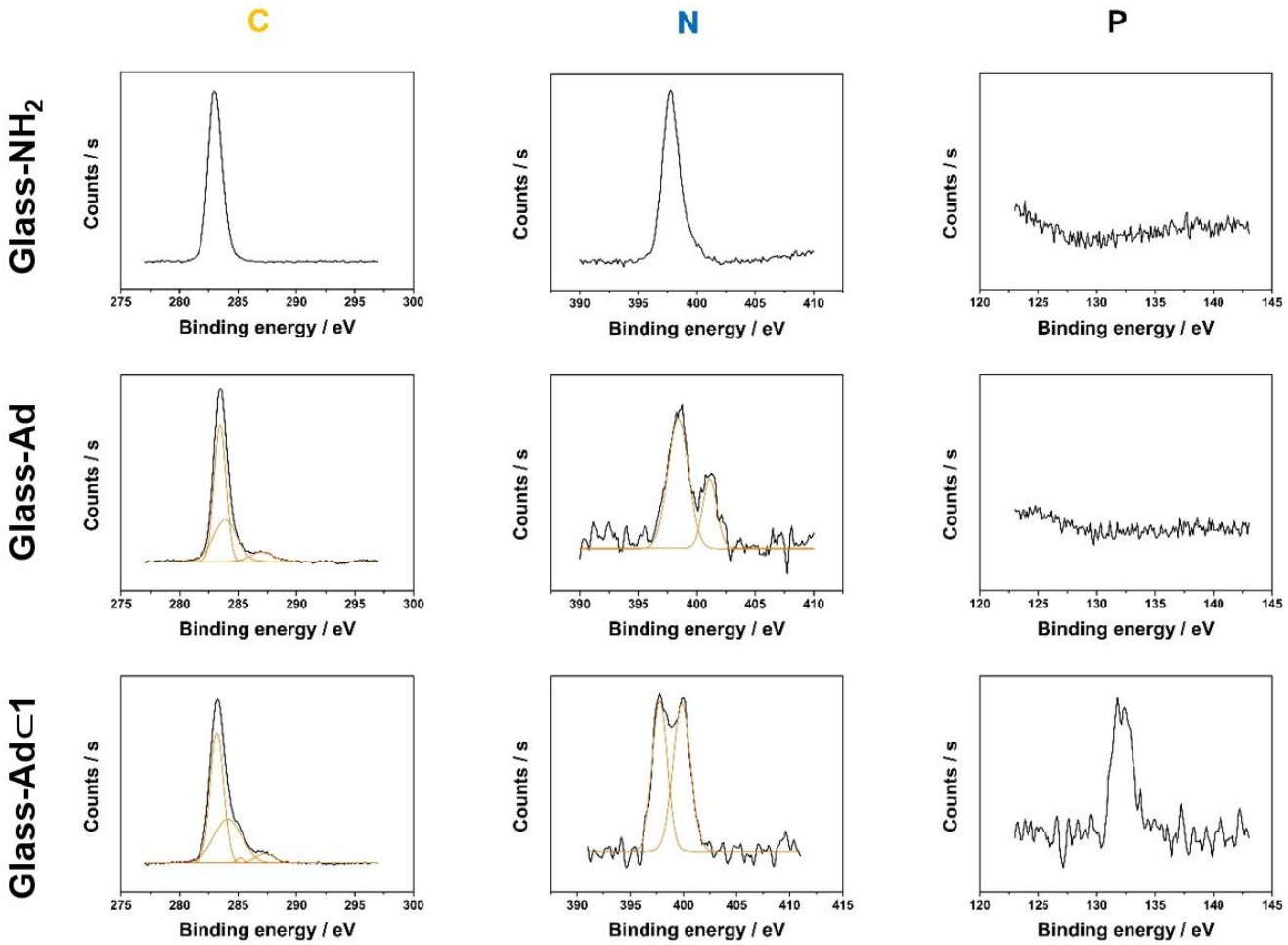

Figure S17. XPS spectra of aminated (Glass-NH_2), Ad-coated (Glass-Ad) and polymer-coated (Glass-Ad⊂1) glass slides.

10. Adhesive Force Measurements using β-CD-Coated AFM Tips

To measure adhesive forces, a single approach–retract cycle was carried out. The AFM probe first approaches the surface from a distance of 2 μm from the surface and the approach continues for another 1.5 μm after contact between the probe and surface. Subsequently, the probe is retracted slowly back to the inital position. The adhesive force between the β-CD-coated AFM probe and different surfaces under water was calculated by subtracting the original adhesive force before contact from the maximum adhesive force during the retracting process (see Figure S18).

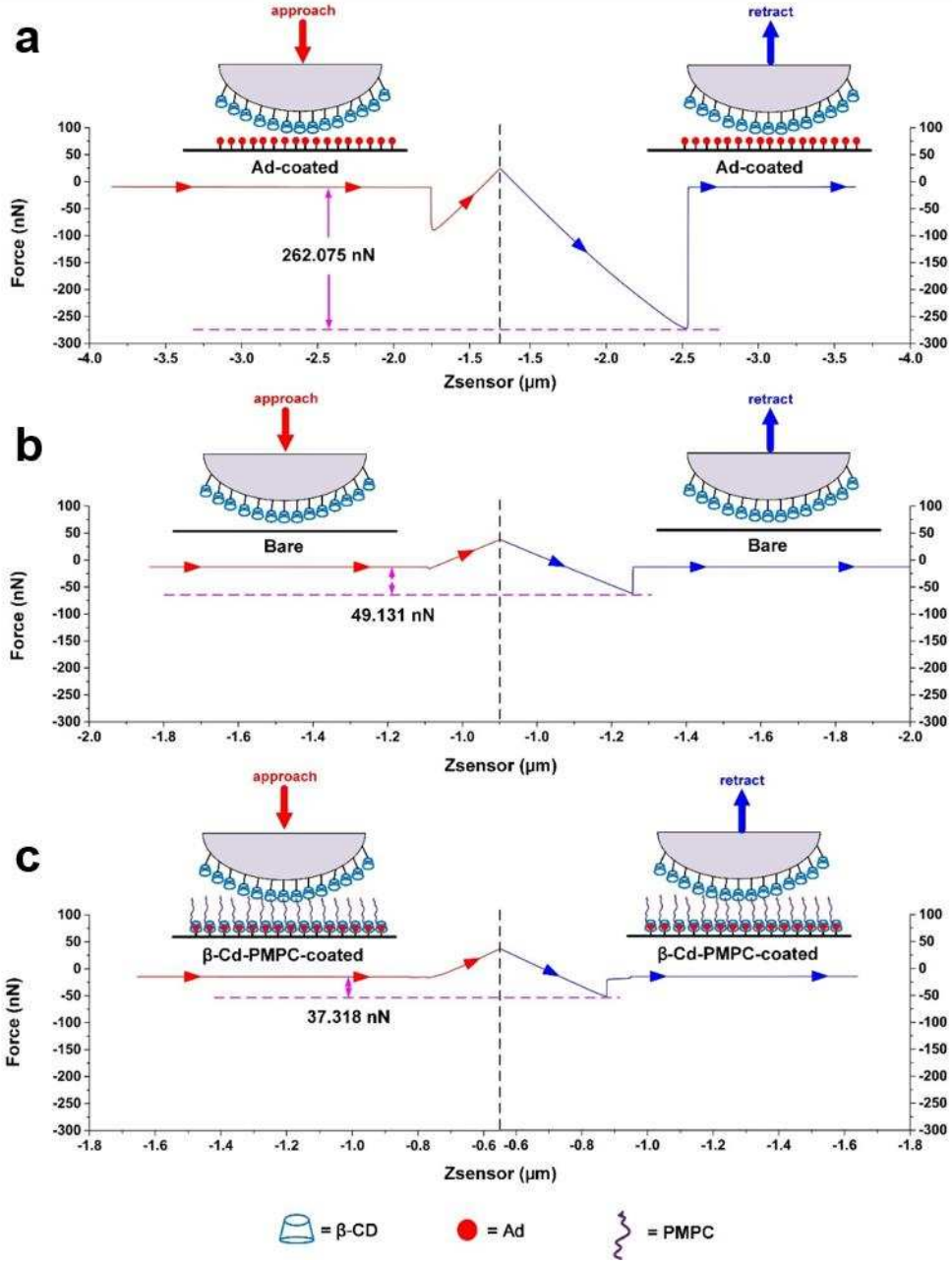

Figure S18. Adhesive force between β-CD-coated AFM tips and (a) bare Ti alloy, (b) Ti-Ad and (c) Ti-Ad⊂1

11. AFM Analysis of Surface Morphology

We examined the roughness of the Ti surfaces and an unfunctionalized glass slide by AFM, quantifying (Figures S19–23) the arithmetic average of the absolute values of the surface height deviations measured from the mean plane (R_a) and the root mean square average of height deviations taken from the mean image data plane (R_q). Measurements were performed in tapping mode under H_2O. The higher deviation in roughness of the bare Ti surface relative to the functionalized surfaces is consistent with the larger error observed in friction measurements (Figure 3) for this surface.

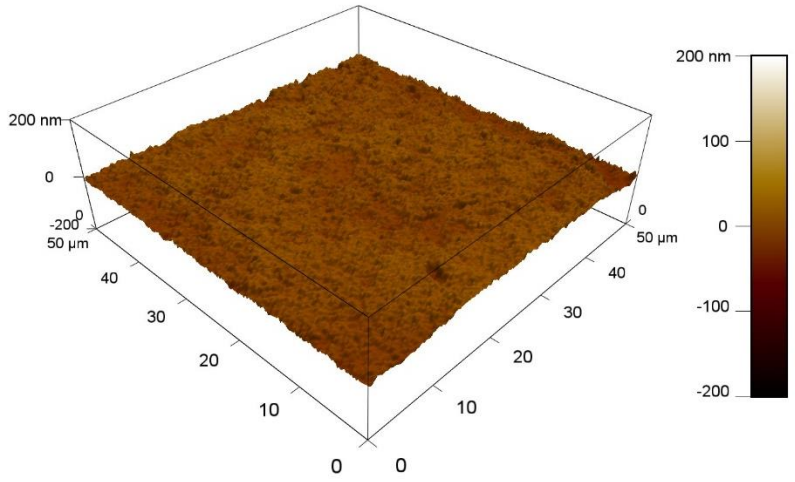

Figure S19. AFM morphology of the bare Ti surface, R_a = 6.718 nm, R_q = 7.654 nm

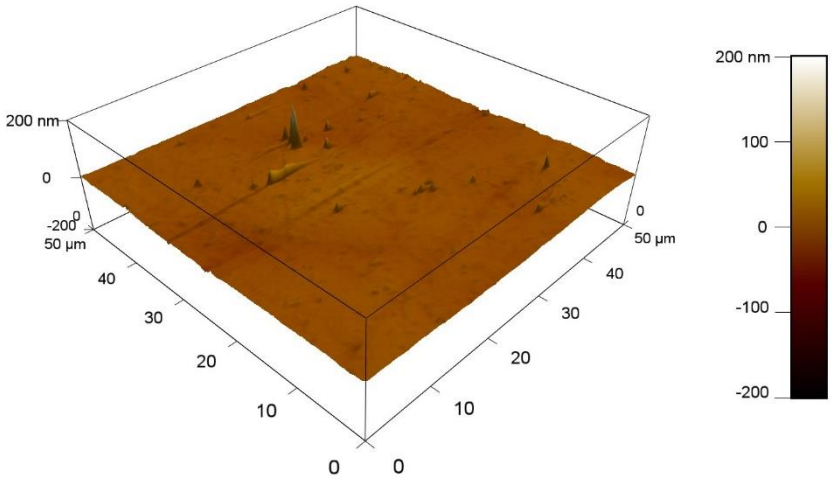

Figure S20. AFM morphology of the Ti-NH_2 surface, R_a = 3.516 nm, R_q = 5.127 nm

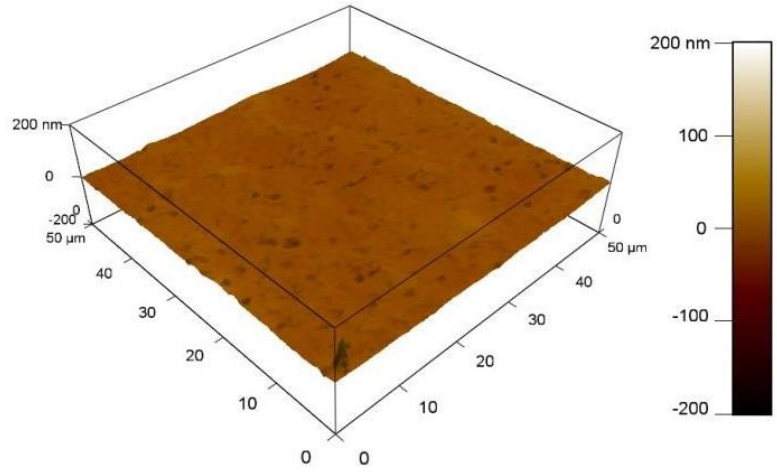

Figure S21. AFM morphology of the Ti-Ad surface, R_a = 3.196 nm, R_q = 4.303 nm

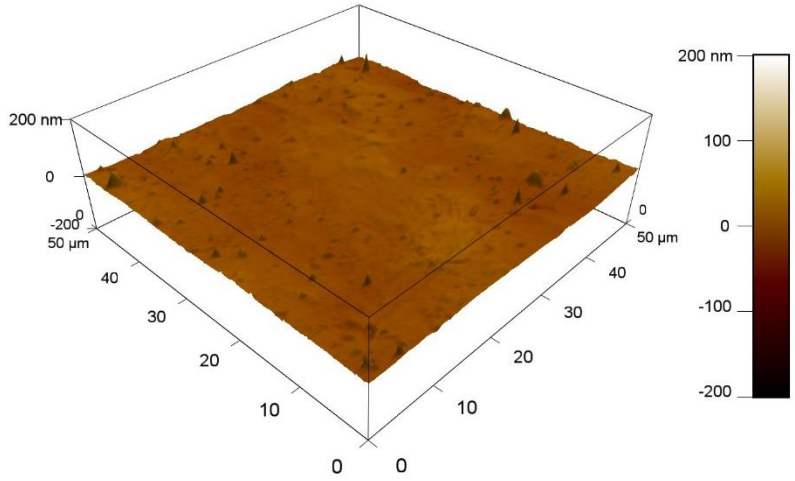

Figure S22. AFM morphology of the Ti-Ad⊂1 surface, R_a = 4.461 nm, R_q = 5.754 nm

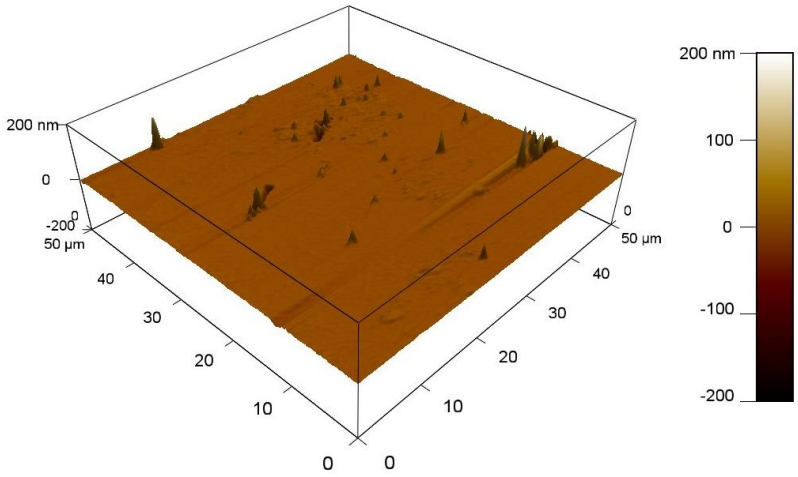

Figure S23. AFM morphology of a glass slide, R_a = 2.113 nm, R_q = 6.494 nm

12. Effect of CD-PMPC 1 Concentration on COF

We examined the effect of concentration of **1** on the surface lubricity. Three **Ti-Ad** wafer surfaces prepared as described in the Materials and Methods section of the manuscript were immersed 2, 10, or 12 mg/mL aqueous solutions of **1**, respectively, to preform three **Ti-Ad⊂1** wafers. Each wafer was immersed for 12 h before rinsing with ultrapure water. Then an AFM friction test was performed under an aqueous solution of **1** at the same concentration used to preform the self-assembled surface layer, i.e., 2, 10, or 12 mg/mL. A PMPC-coated AFM tip was used as shown in Figure 3, inset. AFM fiction measurements (Table S4) were carried out using a sliding area of 20 μm × 20 μm, sliding rate of 2 Hz, a load of 400 nN and 64 scans per area.

Table S4 | Friction force performances measured by AFM in contact mode show the effect of the concentration of **1** on the COF observed for a self-assembled surface of the polymer on **Ti-Ad**.[a]

Entry	[**1**] mg/mL	COF	Standard Deviation
1	2	0.094	0.009
2	10	0.084	0.003
3	12	0.079	0.002

[a] COFs were measured under a load of 400 nN

A relatively small variation in COF is observed across the three concentrations, illustrating that the self-assembled surface forms effectively at concentrations below the standard 10 mg/mL used for experiments in the manuscript. However, there is a small trend toward lower COF with increasing concentration of **1**. Aqueous solutions of **1** approach the solubility limit just above 10 mg/mL and become significanltly more viscous. Consequently, 10 mg/mL was chosen as the most appropriate concentration to investigate the supramolecular repair behaviour of the hydration lubrication surface.

13. Exchange of 1 and 1′ on Glass-Ad in the Absence of Wear

(1) To confirm whether the self-assembled **Glass-Ad⊂1** and **Glass-Ad⊂1′** undergo dynamic exchange rather than friction-induced degradation and (2) to observe this background exchange process, we allowed wafers to equilibrate in the absence of wear. One glass wafer was immersed in 10 mg/mL aqueous solution of **1** for 12 h, then dried under nitrogen flow before subsequently immersing half of the wafer in the 10 mg/mL aqueous solution of **1′** for 12 h (Figure S24a). A second glass wafer was exposed to the polymers in the reverse order. The wafer was immersed in 10 mg/mL aqueous solution of **1′** for 12 h, then dried under nitrogen flow before subsequently immersing half of the wafer in the 10 mg/mL aqueous solution of **1** for 12 h (Figure S24b). In both cases, confocal laser scanning microscopy revealed that the end of the glass slide immersed in the second solution of polymer underwent dynamic exchange.

Contrasting these results with those shown in Figure 4, it is evident that mechanical wear of the surface for 20 min accelerates exchange of the polymer without significant irreversible degradation of the surface. The worn areas in Figure 4 exhibit a large change (decrease or increase) in fluorescence, which, when viewed by CLSM, eclipses the smaller proportion of exchange that has occurred in other areas of the slide during the short, 2 hour equilibration used in that experiment. The background exchange is more easily observed (Figure S24) following the 12 h exchange experiment and without the presence of a worn patch to dominate the colour contrast.

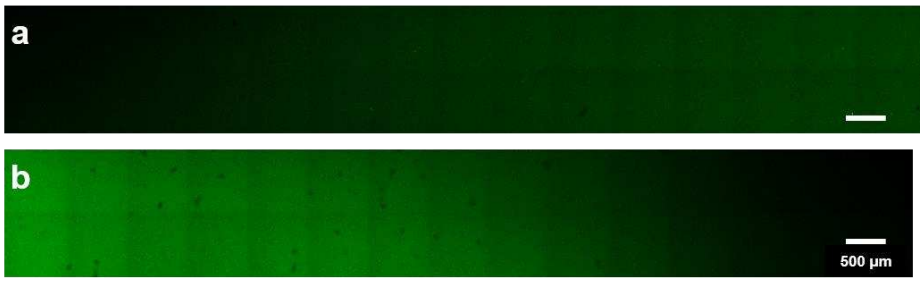

Figure S24. Confocal laser scanning microscope images of glass slides. a A **Glass-Ad⊂1** wafer after immersing the right-hand side in **1′**$_{(aq)}$, and **b** a **Glass-Ad⊂1′** wafer after immersing the right-hand side in **1**$_{(aq)}$. Both slides show exchange of the self-assembled polymer layer. The **Glass-Ad⊂1** slide that had been immersed in **1′**$_{(aq)}$ became emmisive, while the end of the **Glass-Ad⊂1′** slide immersed in **1**$_{(aq)}$ became non-emmisive.

14. Quartz Crystal Microbalance Data

The surface adsorption of polymer **1** was examined by quartz crystal microbalance (QCM). The instrument used was a Q Sense Explorer, Biolin Scientific, Sweden. We first prepared appropriately functionalised QCM sensors; the gold surfaces of QSense Gold sensors were sputtered with Ti using a sputter meter (JS-3, Institute of Microelectronics of the Chinese Academy of Sciences, China) to produce a layer of 15 nm thickness. To obtain a Ad-functionalised chip (**Ti-Ad**), the Ti-surface of the chip was then treated with 100 μL of *N*-[3-(triethoxysilyl)propyl)adamantane-1-carboxamide solution (72% ethanol, 8% water, 20% *N*-[3-(triethoxysilyl)propyl)adamantane-1-carboxamide, v/v/v) at room temperature. After 12 h, the chip was rinsed repeatedly with ultrapure water to remove any unbound materials, before drying the surface under a stream of N_2. The QCM adsoption data for the functionalised **Ti-Ad** chip and the bare Ti chip in a solution of $\mathbf{1}_{(aq)}$ are shown in Figure 5c,d.

The Sauerbrey equation below was used to derive the mass densities following treatment with the polymer solution and subsequent rinsing with water:

$$\Delta m = \Delta f \cdot \frac{17.7}{n}$$

Where Δm is the change in mass per unit area and n is overtone of the frequency used (here n = 3).

The final adsorption capacity of these two surfaces is different as evident by the differences in $\Delta f_{solution}$, Δf_{rinsed}, and the corresponding mass densities, $\Delta m_{solution}$, Δm_{rinsed}, given in Table S5.

Table S5 | Mass densities measured by QCM for self-assembly of polymer **1** on bare Ti and **Ti-Ad**.

Surface	$\Delta m_{solution}$ ng·cm^{-1}	Δm_{rinsed} ng·cm^{-1}	Percentage retained
Ti	782.6	512.3	65%
Ti-Ad	981.4	856.5	87%

We note that the Sauerbrey equation is most accurate for a ultrathin, compact surface layer that is solvent free.[S4] The adsorbed polymer **1** is infused with solvent and will have viscoelastic character, so this method may overestimate the mass absorbed and should be interpreted as an upper limit. However, the comparison of Ti and **Ti-Ad** by QCM reveals the following insights. The adsorption capacity of the **Ti-Ad** surface for **1** is greater than bare Ti (Figure 5c and Table S5), which is consistent with the formation of a stronger interaction between the polymer and the surface, i.e., the specific noncovalent interaction of the β-CD and Ad groups. Similarly, upon rinsing the equilibrated suraces with water, a greater mass of polymer desorbs from the Ti surface, confirming the increased relative stability of the **Ti-Ad⊂1** self-assembled coating. After rinsing **Ti-Ad⊂1** with water for ~6000 s, 87% of the polymer by mass is retained on the surface, whereas only 65% of the polymer mass is retained after the Ti surface has been rinsed for ~3750 s. The differing kinetics of the two systems is also evident from the QCM data (Figure 5c,d). Polymer **1** adsorbs to the **Ti-Ad** surface at a higher rate initially, as shown by comparing differentials of the Δ*f* curves (Figure 5d). The peak rates of adsorbtion of **1** were obserevd at ~10 s for **Ti-Ad** and ~25 s for the bare Ti surface. The peak rate of **Ti-Ad** is ~3 times that of bare Ti. Again, this is consistent with the **Ti-Ad** surface exhibiting a higher association constant with **1** than bare Ti and, by corollary, a faster rate of association and/or slower rate of dissociation ($K_a = \frac{k_{on}}{k_{off}}$). A lower k_{off} for **Ti-Ad⊂1** also fits with the longer period required for its surface coating to equilibrate fully. A plateau in the frequency of the **Ti-Ad** chip is observed after <2000 s in the presence of $\mathbf{1}_{(aq)}$, whereas the bare Ti chip requires ~4000 s. Overall, therefore, it appears that polymer **1** rapdily coats the **Ti-Ad** surface – a majority (>66%) of the eventual surface mass is deposited within 2 minutes. But a longer time is required to achieve a saturated monolayer at equilibrium – the frequency continues to decrease slowly up to 30 minutes.

We observe 981.4 ng·cm^{-2} of polymer **1** on the **Ti-Ad** surface. Applying the M_W of **1** (540 kDa) measured by DOSY NMR (Table S1), this value corresponds to a molar density of 1.82 pmoles·cm^{-2}. For context, this value is a factor of 10 lower than a close packed monolayer of a hexanethiol 12-mer oligonucleotides on a gold film.[S5] In that system, a coverage of 18 pmoles·cm^{-2} is measured, giving a reasonable upper limit of what coverage could reasonably be expected. Given that (i) one in three of the surface NH_2 sites are functionalised with an Ad group on the **Ti-Ad** surface (Figure 2) and (ii) the footprint of self-assembling group (Ad–β-CD) is rather more bulky than a thiol–gold interaction on account of the large CD headgroup and the (likely mixture of mushroom-like and brush-like) polymer structure, this value of 1.82 pmoles·cm^{-2} is indicative of a relatively closely packed, complete monolayer structure at equilibrium.

15. Supplemental References

S1. Timoshenko S. & Goodier J.N. (1970). Theory of Elasticity (McGraw-Hill).

S2. Martienssen, W. & Warlimont, H. (Eds.). (2005) Springer Handbook of Condensed Matter and Materials Data (Springer).

S3. Vafaeian, B., et al. Hip joint contact pressure distribution during Pavlik harness treatment of an infant hip: A patient-specific finite element model. (2018) J. Biomech. Eng. *140*, 071009.

S4. Lee, H. S. & Penn, L. S. In situ study of polymer brushes as selective barriers to diffusion. (2008) Macromolecules *41*, 8124.

S5. Demers, L. M., et al. A fluorescence-based method for determining the surface coverage and hybridization efficiency of thiol-capped oligonucleotides bound to gold thin films and nanoparticles. (2000) Anal. Chem. *72*, 5535.